66 $(CH_3)_3NCH_2COO \cdot CaCl_2 \cdot 2H_2O$

66A Pure compound

No. 66A-1 $(CH_3)_3NCH_2COO \cdot CaCl_2 \cdot 2H_2O$, Betaine calcium chloride dihydrate (BCCD)

(M = 264.16; [D: 279.25])

1a Ferroelectricity in $(CH_3)_3NCH_2COO \cdot CaCl_2 \cdot 2H_2O$ was reported by Rother et al. in 1984. 84Rot

b

phase	II	modulated phases *	I	84Rot
state	F		P	
crystal system	orthorhombic		orthorhombic [a])	[a]) 85Bri2
space group			Pnma – D_{2h}^{16} [a])	
Θ [K]	Θ_f = 46 [b])		Θ_i = 164	[b]) 91Rib1

* Phases with modulated structures characterized by modulation vectors || to the c* axis [85Bri1].

See also subsection 14a.

Dielectric anomalies were observed at Θ_i = 164 K, 127 K, 125K, 116 K, 75 K, 51 K, 47 K and 43 K [a]), and at 115 K, 114 K, 77 K, 76 K, 55 K and 46 K [b]). [a]) 84Rot [b]) 91Rib1

See also subsection 5a.

Multiple hysteresis loops were observed between 125 K and 51 K. 84Rot

See also subsection 5c.

$\Theta - p$ phase diagram: see Fig. 66A-1-037, Fig. 66A-1-038, Fig. 66A-1-039 in subsection 5a and Fig. 66A-1-085 in subsection 14b.

$\Theta - E$ phase diagram: see Fig. 66A-1-086 in subsection 14b.

Crystal system and space group: orthorhombic, Pnma – D_{2h}^{16} at RT; 84Rot, 85Bri2

orthorhombic, $P2_1ca - C_{2v}^5$ at 90 K. 92Ezp

Wave vectors and direction of P_s of modulated phases: Table 66A-1-001; see also subsection 14a.

P_s || [010] below Θ_f: see also subsection 5c. 84Rot

$\rho = 1.460(2) \cdot 10^3$ kg m^{-3}. 84Rot

$\rho = 1.46 \cdot 10^3$ kg m^{-3}, $\rho_X = 1.457 \cdot 10^3$ kg m^{-3} at RT. 85Bri2

$\rho_X = 1.49 \cdot 10^3$ kg m^{-3} at 90 K. 92Ezp

Transparent, colorless. 84Rot

Cleavage plane: (010), (011). 84Rot

2a Crystal growth: evaporation from aqueous solution. 84Rot

3a Unit cell parameters:

a = 10.97 Å, b = 10.15 Å, c = 10.82 Å at RT. 85Bri2

a = 10.894(2) Å, b = 10.013(1) Å, c = 43.237(6) Å at 90 K. 92Ezp

For averaged structure of modulated structure with $\boldsymbol{q} = 0.296\ \boldsymbol{c}^*$ at 130 K: 91Zun

a = 10.909(7) Å, b = 10.029(3) Å, c = 10.813 Å.

b Z = 4 at RT. 85Bri2

Z = 16 at 90 K. 92Ezp

Crystal structure: Fig. 66A-1-001, Fig. 66A-1-002, Fig. 66A-1-003.

Fractional coordinates and temperature parameters: Table 66A-1-002, Table 66A-1-003, Table 66A-1-004.
Interatomic distances and angles: Table 66A-1-005.
Parameters of modulated structures: Table 66A-1-006, Table 66A-1-007.

4 Lattice distortion: see 85Bri1

5a Dielectric constant and dielectric loss:
along the *b* axis: Fig. 66A-1-004, Fig. 66A-1-005, Fig. 66A-1-006, Fig. 66A-1-007, Fig. 66A-1-008, Fig. 66A-1-009, Fig. 66A-1-010, Fig. 66A-1-011, Fig. 66A-1-012, Fig. 66A-1-013, Fig. 66A-1-014, Fig. 66A-1-015, Fig. 66A-1-016, Fig. 66A-1-017, Fig. 66A-1-018, Fig. 66A-1-019.
along the *a* or *c* axis: Fig. 66A-1-020, Fig. 66A-1-021, Fig. 66A-1-022, Fig. 66A-1-023.
Effect of doping of Mn or Br: Fig. 67A-1-024, Fig. 66A-1-025, Fig. 66A-1-026, Fig. 66A-1-027, Fig. 66A-1-028, Fig. 66A-1-029, Fig. 66A-1-030, Fig. 66A-1-031.
Effect of hydrostatic pressure: Fig. 66A-1-032, Fig. 66A-1-033.
Effect of shear stress T_{13}: see Fig. 66A-1-019.
Dielectric dispersion: Fig. 66A-1-034, Fig. 66A-1-035.
Relaxation time: Fig. 66A-1-036.
$\Theta - p$ phase diagram: Fig. 67A-1-037, Fig. 66A-1-038, Fig. 66A-1-039.
$\Theta - T_{13}$ phase diagram: Fig. 66A-1-040.
$\Theta - E$ phase diagram: Fig. 66A-1-041.

b Effect of E_{bias} on κ: Fig. 66A-1-042, Fig. 66A-1-043, Fig. 66A-1-044, Fig. 66A-1-045, Fig. 66A-1-046, Fig. 66A-1-047, Fig. 66A-1-048.
Effect of signal field strength: Fig. 66A-1-049.

c *P–E* hysteresis loop: Fig. 66A-1-050.
Spontaneous polarization, induced polarization, coercive field and critical field: Fig. 66A-1-051, Fig. 66A-1-052, Fig. 66A-1-053, Fig. 66A-1-054, Fig. 66A-1-055, Fig. 66A-1-056, Fig. 66A-1-057, Fig. 66A-1-058, Fig. 66A-1-059, Fig. 66A-1-060.

d Pyroelectric coefficient: Fig. 66A-1-061, Fig. 66A-1-062, Fig. 66A-1-063; see also Fig. 66A-1-006, Fig. 66A-1-022 in subsection 5a and Fig. 66A-1-054, Fig. 66A-1-057, Fig. 66A-1-058, Fig. 66A-1-059, Fig. 66A-1-060 in subsection 5c and 88Rib1

6a Specific heat: Fig. 66A-1-064.
Transition heat and transition entropy: 90Bri

Θ [K]	ΔQ_m [J mol^{-1}]	ΔS_m [J mol^{-1} K^{-1}]
47	5.08(15)	0.11(1)
76	11.90(36)	0.16(2)
116	5.60(17)	0.050(5)
127	1.58(15)	0.010(2)
164	187.4(56)	1.28(6)

See also 84Rot

8a Elastic stiffness: Table 66A-1-008; Fig. 66A-1-065.
Ultrasonic velocity and attenuation: Fig. 66A-1-066, Fig. 66A-1-067, Fig. 66A-1-068, Fig. 66A-1-069.

9a Refractive indices at 589 nm: $n_\alpha = 1.489(2)$ ($\boldsymbol{E} \parallel [010]$), $n_\beta = 1.531$ (2) ($\boldsymbol{E} \parallel [001]$), $n_\gamma = 1.552(2)$ at 293 K. 84Rot
Rotation angle of optical indicatrix: Fig. 66A-1-070.
Birefringence: Fig. 66A-1-071, Fig. 66A-1-072; see also 90Kro, 95Sve
Far-infrared spectra: Table 66A-1-009; Fig. 66A-1-073, Fig. 66A-1-074; see also 88AoR1

10a Raman scattering: Fig. 66A-1-075, Fig. 66A-1-076, Fig. 66A-1-077;
see also 91Wil, 94Ill

13a NMR of ^2H in D_2O:
EFG tensor component [kHz]; $V_{xx} = 138$, $|V_{xy}| = 41$, $|V_{xz}| = 48$, $V_{yy} = -138$, $|V_{yz}| = 94$, $V_{zz} = 0$ with principal axes of the unit vectors $\boldsymbol{e_1} = (0.89, 0.24, 0.38)$, $\boldsymbol{e_2} = (-0.45, 0.37, 0.81)$, $\boldsymbol{e_3} = (0.05, -0.90, 0.44)$. 92Hac
NMR of ^{35}Cl:
EFG tensor component [kHz]; $V_{xx} = 946$, $V_{xy} = 1263$, $V_{xz} = 1866$, $V_{yy} = -491$, $V_{yz} = 4090$, $V_{zz} = -455$ with principal axes of the unit vectors $\boldsymbol{e_1} = (0.4929, 0.5981, 0.6319)$, $\boldsymbol{e_2} = (-0.0848, -0.6898, 0.719)$, $\boldsymbol{e_3} = (-0.866, 0.408, 0.2892)$. 95Hol

b ESR of Mn^{2+} doped BCCD: see 88Rib2, 90Eme, 92Hei
ESR of Mn^{2+} and VO^{2+} doped BCCD: see 89Fuj
ESR of γ-irradiated BCCD: see 91Met

14a Modulation wave vector δ relative to c^* between about 80 K and 164 K: 95Kia

Θ [K]	≤80	≥115	117.3	119.5	124	126.8	164
δ	2/9	1/4	4/15	3/11	IC *	2/7	IC *	1

* Incommensurately modulated structure.

See also Table 66A-1-001 in subsection 1b.
X-ray satellite reflections: Fig. 66A-1-078, Fig. 66A-1-079.
$I \approx (\Theta_i - T)^{2\beta}$, $\Theta_i = 164$ K, $2\beta = 0.85$ at $(0, 8, \bar{2} + \delta)$ and $(0, 6, \delta)$. 85Bri1
Temperature dependence of satellite intensities I:
Neutron satellite scattering: Fig. 66A-1-080, Fig. 66A-1-081, Fig. 66A-1-082, Fig. 66A-1-083, Fig. 66A-1-084.
$\Theta - p$ phase diagram: Fig. 66A-1-085. $\Theta - E$ phase diagram: Fig. 66A-1-086.

b Neutron inelastic scattering: Fig. 66A-1-087, Fig. 66A-1-088, Fig. 66A-1-089, Fig. 66A-1-090.

Table 66A-1-001. $(CH_3)_3NCH_2COO \cdot CaCl_2 \cdot 2H_2O$ (BCCD), $(CD_3)_3NCD_2COO \cdot CaCl_2 \cdot 2D_2O$ (DBCCD). Wave vector of modulation δ relative to c^*, temperature range of stability of the corresponding modulated structure, $T_1 - T_2$, and direction of the spontaneous polarization [92Alm]. Column 2: dielectric data in [89Unr]. Column 4: X-ray data in [85Bri1]. Column 5: dielectric data in [92Cha]. See also subsection 14b.

$\delta = m/n$	$T_1 - T_2$ [K]	Direction	$T_1 - T_2$ [K]	
	BCCD	of P_s	BCCD	D-BCCD
2/7	127.8–124.5	***b***	127–125	130–127
3/11	118.4–117.4	(0)		
4/15	116.0–115.7	***b***		
6/23	115.4	***b***		
1/4	115.3–75.8	***a***	116–73	116.9–79.2
2/9	75.8–75.2	***b***		
1/5	75.2–53.3	(0)	73–53	79.2–56.5
2/11	53.3–53.0	***b***		
1/6	53.0–47.1	***a***	53–47 and < 43	56.5–49.8
2/13	47.1–46.9	***b***		
1/7	46.9–46.2	(0)		
1/8	46.2–46.0	***a***		
1/1	46.0 and below	***b***	47–43	49.8 and below

Table 66A-1-002. $(CH_3)_3NCH_2COO \cdot CaCl_2 \cdot 2H_2O$ (BCCD). Fractional coordinates and anisotropic temperature parameters U_{ij} [$Å^2$] at RT [85Bri2]. U_{ij} is defined by Eq. (d) in Introduction.

	x	y	z	U_{11}	U_{22}	U_{33}	U_{12}	U_{13}	U_{23}
Ca	0.19515(7)	0.25	0.22395(7)	0.0213(4)	0.0369(4)	0.0232(4)	0	–0.0037(4)	0
Cl	0.30459(6)	0.44590(7)	0.08777(6)	0.0405(4)	0.0459(4)	0.0479(5)	–0.0089(4)	–0.0036(4)	0.0123(4)
O(3)	0.0909(2)	0.4050(2)	0.3504(2)	0.037(1)	0.079(2)	0.052(2)	+0.011(1)	0.000(1)	–0.028(1)
O(1)	0.5374(2)	0.25	0.4114(2)	0.024(1)	0.081(2)	0.034(2)	0	+0.007(1)	0
O(2)	0.3417(3)	0.25	0.3675(3)	0.039(2)	0.123(3)	0.044(2)	0	–0.020(2)	0
C(4)	0.4281(4)	0.25	0.4391(4)	0.032(2)	0.039(2)	0.030(3)	0	–0.003(2)	0
C(3)	0.3888(3)	0.25	0.5745(4)	0.027(2)	0.044(3)	0.036(3)	0	0.002(2)	0
N	0.4868(3)	0.25	0.6705(3)	0.037(2)	0.076(3)	0.0236(2)	0	0.006(2)	0
C(1)	0.4262(6)	0.25	0.7958(5)	0.069(4)	0.108(6)	0.0355(3)	0	0.022(3)	0
C(2)	0.5630(5)	0.3713(7)	0.6612(5)	0.088(4)	0.152(5)	0.057(3)	–0.082(4)	0.027(3)	–0.43(3)
H(1)	0.381(2)	0.328(2)	0.801(2)	0.06(1)					
H(2)	0.503(5)	0.25	0.863(5)	0.17(3)					
H(3)	0.609(4)	0.386(5)	0.735(4)	0.18(2)					
H(4)	0.505(4)	0.447(5)	0.656(5)	0.19(3)					
H(5)	0.606(3)	0.367(3)	0.586(3)	0.08(1)					
H(6)	0.343(2)	0.334(2)	0.567(2)	0.052(8)					
H(7)	0.018(3)	0.407(3)	0.366(3)	0.09(1)					
H(8)	0.124(3)	0.444(4)	0.416(3)	0.13(2)					

Table 66A-1-003. $(CH_3)_3NCH_2COO \cdot CaCl_2 \cdot 2H_2O$ (BCCD). Fractional coordinates and mean square displacements $\overline{u^2}$ at T = 130 K [91Zun]. For non-hydrogen atoms, the mean square displacements are reduced by $\overline{u^2} = (U_{11} + U_{22} + U_{33})/3$, where U_{ij} is defined by Eq. (d) in Introduction.

Atom	x	y	z	$\overline{u^2}$ [Å^2]
Ca	0.1935(1)	0.2500	0.2246(1)	0.0174(3)
Cl	0.3042(1)	0.4469(1)	0.0881(1)	0.0258(3)
C1	0.4311(4)	0.2500	0.7931(6)	0.053(2)
C2	0.5649(2)	0.3725(3)	0.6590(3)	0.048(1)
C3	0.3892(3)	0.2500	0.5786(4)	0.018(1)
C4	0.4265(2)	0.2500	0.4438(4)	0.016(1)
N	0.4889(2)	0.2500	0.6705(4)	0.017(1)
O1	0.5351(2)	0.2500	0.4117(3)	0.022(1)
O2	0.3374(2)	0.2500	0.3715(3)	0.038(1)
O3	0.0890(1)	0.4077(2)	0.3498(2)	0.035(1)
H1	0.3835(28)	0.3233(33)	0.7952(32)	0.050
H2	0.4988(42)	0.2500	0.8675(48)	0.050
H3	0.6182(35)	0.3753(43)	0.7261(50)	0.050
H4	0.5009(28)	0.4655(26)	0.6628(35)	0.050
H5	0.6044(28)	0.3693(34)	0.5839(22)	0.050
H6	0.3390(25)	0.3196(26)	0.5796(31)	0.050
H7	0.0075(19)	0.4164(34)	0.3679(25)	0.050
H8	0.1246(24)	0.4394(33)	0.4179(23)	0.050

Table 66A-1-004. $(CH_3)_3NCH_2COO \cdot CaCl_2 \cdot 2H_2O$ (BCCD). Fractional coordinates and mean square displacements $\overline{u^2}$ at T = 90 K [92Ezp]. For Ca, Cl, N and O atoms, the mean square displacements are reduced by $\overline{u^2} = (U_{11} + U_{22} + U_{33})/3$, where U_{ij} is defined by Eq. (d) in Introduction.

Atom	x	y	z	$\overline{u^2}$ [Å^2]
Ca1	0.19165(6)	0.26010(6)	–0.00642(2)	0.0083
N1	0.4905(2)	0.2355(3)	0.10517(8)	0.0145
O11	0.5336(2)	0.2425(2)	0.04047(7)	0.0120
O21	0.3355(2)	0.2776(3)	0.03123(7)	0.0167
Cl1	0.30292(9)	0.45040(8)	–0.04266(2)	0.0157
Cl4	0.29979(8)	0.05609(9)	–0.03846(2)	0.0159
O31	0.0857(2)	0.4251(3)	0.02325(7)	0.0251
O34	0.0870(2)	0.1083(3)	0.02672(6)	0.0186
Ca3	0.19179(7)	0.24065(6)	0.24386(2)	0.0107
N3	0.4890(2)	0.2202(2)	0.35483(7)	0.0128
O13	0.5340(2)	0.2385(2)	0.29068(7)	0.0139
O23	0.3394(2)	0.2619(3)	0.27945(8)	0.0257
Cl5	0.29132(8)	0.44788(9)	0.20968(2)	0.0138
Cl8	0.31461(7)	0.05426(9)	0.20898(2)	0.0131
O35	0.0763(2)	0.3796(3)	0.27703(6)	0.0147
O38	0.0988(2)	0.0650(3)	0.27247(7)	0.0200
Ca2	0.30542(7)	0.74901(7)	0.11881(2)	0.0120
N2	0.0103(2)	0.7228(3)	0.23102(8)	0.0128
O12	0.9650(2)	0.7442(3)	0.16507(8)	0.0186
O22	0.1625(2)	0.7740(3)	0.15532(9)	0.0214
Cl2	0.18472(9)	0.55790(9)	0.08534(2)	0.0173
Cl3	0.20106(8)	0.95091(8)	0.08354(2)	0.0128
O32	0.4022(2)	0.5809(3)	0.14886(7)	0.0196
O33	0.4168(2)	0.8959(3)	0.15079(7)	0.0181
Ca4	0.80475(6)	0.73732(6)	0.13146(2)	0.0081
N4	0.5107(2)	0.7304(3)	0.01950(8)	0.0169
O14	0.4615(2)	0.7420(3)	0.08440(8)	0.0190
O24	0.6668(2)	0.7573(3)	0.09379(8)	0.0226
Cl6	0.70484(8)	0.94709(9)	0.16454(2)	0.0154
Cl7	0.68426(8)	0.55186(9)	0.16622(2)	0.0167
O36	0.9177(2)	0.8808(3)	0.09770(7)	0.0216
O37	0.9016(2)	0.5651(3)	0.10185(6)	0.0123
C11	0.4284(2)	0.2359(3)	0.1369(1)	0.0129
C31	0.3910(2)	0.2550(3)	0.08293(8)	0.0085
C41	0.4232(2)	0.2587(3)	0.04828(7)	0.0022
C21	0.5764(2)	0.3541(4)	0.10410(8)	0.0135
C24	0.5523(2)	0.1036(4)	0.10014(9)	0.0140
C13	0.4406(2)	0.2236(4)	0.38751(9)	0.0131
C33	0.3891(2)	0.2590(3)	0.33273(9)	0.0121
C43	0.4262(2)	0.2536(3)	0.2979(1)	0.0162
C25	0.5840(2)	0.3304(4)	0.3550(1)	0.0190
C28	0.5574(2)	0.1001(4)	0.35054(9)	0.0160
C12	0.0729(2)	0.7091(4)	0.26170(9)	0.0143
C32	0.1127(2)	0.7496(3)	0.20629(9)	0.0118
C42	0.0714(2)	0.7539(3)	0.17258(9)	0.0104
C22	0.9611(2)	0.5790(4)	0.22245(8)	0.0109
C23	0.9078(2)	0.8209(4)	0.23135(8)	0.0125
C14	0.5789(2)	0.7218(5)	–0.0112(1)	0.0320
C34	0.6106(2)	0.7385(3)	0.04253(9)	0.0095
C44	0.5757(2)	0.7441(3)	0.0757(1)	0.0185
C26	0.4256(2)	0.8522(5)	0.0204(1)	0.0256
C27	0.4505(2)	0.5874(5)	0.0261(1)	0.0299

Table 66A-1-005. $(CH_3)_3NCH_2COO \cdot CaCl_2 \cdot 2H_2O$(BCCD). Interatomic distances [Å] and angles [°] at RT [85Bri2].

Distance [Å]		Angle [°]	
Ca–O(2)	2.249(3)	O(2)–Ca–O(3)	86.9(1)
Ca–O(1)	2.281(3)	O(2)–Ca–Cl	93.35(8)
Ca–O(3)	2.391(3)	O(3)–Ca–O(3')	82.8(1)
Ca–Cl	2.767(2)	O(3)–Ca–Cl	92.30(9)
Cl–Cl	4.007(4)	O(3)–Ca–Cl'	175.09(7)
O(3)–Cl	3.722(3)	Cl–Ca–Cl'	92.59(8)
O(3)–O(3')	3.170(6)	H(7)–O(3)–H(8)	103.1(31)
O(3)–H(7)	0.82(3)	Ca–O(2)–C(4)	175.3(3)
O(3)–H(8)	0.89(4)	O(2)–C(4)–O(1)	126.7(4)
C(4)–O(2)	1.231(4)	O(2)–C(4)–C(3)	112.9(3)
C(4)–O(1)	1.241(4)	O(1)–C(4)–C(3)	120.4(4)
C(4)–C(3)	1.534(5)	H(6)–C(3)–H(6')	117.9(26)
C(3)–H(6)	1.00(2)	H(6)–C(3)–N	105.5(13)
C(3)–N	1.504(5)	H(6)–C(3)–C(4)	105.5(14)
N–C(2)	1.501(5)	N–C(3)–C(4)	117.7(3)
C(1)–H(1)	0.94(2)	C(2)–N–C(2')	111.3(6)
C(1)–H(2)	1.12(6)	C(2)–N–C(3)	110.9(3)
C(1)–N	1.511(6)	C(2)–N–C(1)	107.9(3)
C(2)–H(3)	0.96(4)	C(3)–N–C(1)	107.9(4)
C(2)–H(4)	1.00(4)	H(1)–C(1)–H(1')	115.3(34)
C(2)–H(5)	0.95(3)	H(1)–C(1)–H(2)	111.5(21)
		H(1)–C(1)–N	106.5(18)
		H(2)–C(1)–N	104.6(28)
		H(5)–C(2)–H(3)	117.5(30)
		H(5)–C(2)–H(4)	107.7(36)
		H(3)–C(2)–H(4)	105.8(37)
		Ca*–O(1)–C(4)	153.8(3)

' Symmetry code x, $1/2 - y$, z.
* Symmetry code $1/2 + x$, y, $1/2 - z$.

Table 66A-1-006. $(CH_3)_3NCH_2COO \cdot CaCl_2 \cdot 2H_2O$ (BCCD). Structure at 90 K refined by using fourdimensional approach with superspace group $P^{Pnma}_{1s\bar{1}}$ ($\boldsymbol{q} = \boldsymbol{c}^*/4$) [92Ezp].

(**a**) Average structure. Fractional coordinates refer to the basic cell. Mean square displacements are reduced by $\overline{u^2} = (U_{11} + U_{22} + U_{33})/3$, where U_{ij} is defined by Eq. (d) in Introduction.

Atom	*x*	*y*	*z*	$\overline{u^2}$ [Å^2]
Ca	0.19342(4)	0.2500	0.22480(4)	0.0097(2)
Cl	0.30413(4)	0.44709(4)	0.08782(4)	0.0151(3)
C1	0.4311(3)	0.2500	0.7972(3)	0.0208(8)
C2	0.5665(2)	0.3713(3)	0.6590(2)	0.0179(7)
C3	0.3893(3)	0.2500	0.5793(2)	0.0126(4)
C4	0.4257(2)	0.2500	0.4427(2)	0.0118(4)
N	0.4898(2)	0.2500	0.6716(2)	0.0075(4)
O1	0.5349(2)	0.2500	0.4115(2)	0.0158(4)
O2	0.3359(2)	0.2500	0.3725(2)	0.0231(7)
O3	0.0887(1)	0.4081(2)	0.3499(1)	0.0168(4)

(**b**) Amplitudes [$\cdot 10^5$] and phases [$\cdot 10^3$] of the modulation structures. Modulation functions are given as $u_i(t) = a_i \cos [2\pi(t + \phi_i)]$, (i = *x*, *y*, *z*).

Atom	a_x	ϕ_x	a_y	ϕ_y	a_z	ϕ_z
Ca	0	0	1373(6)	132(1)	0	0
Cl	1302(5)	271(1)	–401(6)	460(2)	–687(6)	55(1)
C1	0	0	4109(46)	173(2)	0	0
C2	–2447(28)	231(3)	5016(32)	213(1)	–1686(28)	221(3)
C3	0	0	628(35)	–72(9)	0	0
C4	0	0	848(34)	–71(7)	0	0
N	0	0	3604(29)	198(2)	0	0
O1	0	0	1129(25)	265(4)	0	0
O2	0	0	2788(31)	–145(2)	0	0
O3	1126(18)	224(3)	3205(20)	154(1)	–1080(18)	146(3)

Table 66A-1-007. $(CH_3)_3NCH_2COO \cdot CaCl_2 \cdot 2H_2O$ (BCCD). Amplitudes [$\cdot 10^5$] and phases [$\cdot 10^3$] of the modulation structures [91Zun]. T = 130 K. Modulation functions are given as $u_i(t) = a_i \cos [2\pi (t + \phi_i)]$, (i = x, y, z).

Atom	a_x	ϕ_x	a_y	ϕ_y	a_z	ϕ_z
Ca	0	0	975(6)	122(1)	0	0
Cl	877(5)	275(1)	–300(5)	459(3)	–521(8)	62(2)
C1	0	0	2973(58)	152(3)	0	0
C2	–1808(34)	227(3)	3632(46)	205(2)	–1161(43)	210(5)
C3	0	0	543(32)	–63(10)	0	0
C4	0	0	674(31)	–52(7)	0	0
N	0	0	2632(36)	186(2)	0	0
O1	0	0	796(24)	247(5)	0	0
O2	0	0	2071(31)	–129(2)	0	0
O3	740(17)	222(4)	2260(21)	136(1)	–724(22)	117(5)
H1	–2017(373)	183(30)	1604(422)	141(38)	–178(350)	179(300)
H2	0	0	4891(595)	167(17)	0	0
H3	–1146(281)	202(39)	4413(445)	197(15)	–2136(251)	207(18)
H4	–2803(322)	214(18)	2231(277)	207(20)	–199(367)	–228(316)
H5	2282(360)	766(22)	3987(473)	–763(15)	–1221(282)	236(34)
H6	1586(327)	–247(32)	1284(320)	–186(38)	–743(359)	–687(69)
H7	673(237)	–754(56)	1613(336)	143(31)	–1425(296)	126(33)
H8	–631(255)	–143(63)	1306(327)	151(41)	–281(258)	347(153)

Table 66A-1-008. $(CH_3)_3NCH_2COO \cdot CaCl_2 \cdot 2H_2O$ (BCCD). $c_{\lambda\mu}$ vs. T [88Hau]. $c_{\lambda\mu}$: elastic stiffness [$\cdot 10^{10}$ N m^{-2}]. f = 4…40 MHz.

T [K]	c_{11}	c_{22}	c_{33}	c_{44}	c_{55}	c_{66}	c_{12}	c_{13}	c_{23}
293	2.979	1.826	1.919	0.570	0.862	0.312	0.969	1.045	1.401
233	3.027	1.836	1.951	0.589	0.890	0.321	0.976	1.036	1.430
193	3.046	1.824	1.943	0.601	0.909	0.327	0.967	1.008	1.438
177	3.003	1.786	1.886	0.609	0.919	0.331	0.934	0.950	1.418
169	2.850	1.746	1.825	0.612	0.931	0.334	0.888	0.809	1.387
158	2.936	1.788	1.853	0.620	0.938	0.338	0.943	0.839	1.459
143	2.969	1.824	1.877	0.627	0.948	0.341	0.959	0.848	1.474
129	2.997	1.857	1.894	0.638	0.961	0.345	0.972	0.858	1.481
125	3.007	1.870	1.904	0.642	0.965	0.347	0.982	0.859	1.488
117	3.024	1.895	1.927	0.646	0.970	0.349	0.994	0.867	1.502

Table 66A-1-009. $(CH_3)_3NCH_2COO \cdot CaCl_2 \cdot 2H_2O$ (BCCD). Mode frequencies [cm^{-1}] observed in far-IR spectra [93Kam]. vw: very weak, w: weak, m: medium, s: strong, vs: very strong.

E ∥ *a*			***E*** ∥ *b*			***E*** ∥ *c*		
Frequency [cm^{-1}]			Frequency [cm^{-1}]			Frequency [cm^{-1}]		
15 K	170 K	Mode	15 K	170 K	Mode	15 K	170 K	Mode
32 (w)	–	B_{1g}	22 (vw)	–	A_u	31 (w)	(28)	B_{3g}
37 (w)	–	I	31 (vw)	–	A_u	37 (vw)	–	I
43 (w)	?	?	35 (vs)	15	B_{2u}	43 (vw)	–	$L(B_{3u})$
47 (vs)	44	B_{3u}	41 (s)	–	A_g	51 (w)	–	B_{3g}
52 (s)	–	B_{1g}	56 (m)	–	A_g	57 (vw)	–	I
57 (vw)	–	I	60 (w)	?	B_{2u}?	61 (m)	?	B_{1u}
64 (m)	–	B_{1g}	68 (w)	–	A_g	65 (m)	?	B_{1u}
68 (vw)	–	I	76 (m)	?	B_{2u}	74 (w)	–	B_{3g}
77 (m)	?	B_{3u}	87 (w)	–	A_u	88 (m)	86	B_{1u}
82 (w)	?	B_{3u}	104 (m)	–	A_g	93 (w)	–	B_{3g}
86 (w)	–	B_{1g}	109 (s)	107	B_{2u}	106 (vs)	104	B_{1u}
93 (s)	95	B_{3u}	113 (m)	?	B_{2u}	126 (m)	–	B_{3g}
105 (m)	–	B_{1g}	118 (m)	?	B_{2u}	140 (m)	138	B_{1u}
117 (s)	?	B_{3u}	167 (s)	164	B_{2u}	165 (w)	–	B_{3g}
126 (vs)	122	B_{3u}	184 (vs)	179	B_{2u}	179 (vs)	176	B_{1u}
133 (vs)	133	B_{3u}	205 (vs)	202	B_{2u}	203 (s)	?	B_{1u}
137 (vs)	?	B_{3u}	210 (m)	?	B_{2u}	211 (vs)	203	B_{1u}
157 (s)	149	B_{3u}	254 (m)	253	B_{2u}	223 (s)	222	B_{1u}
174 (m)	–	B_{1g}	303 (s)	298	B_{2u}	268 (s)	270	B_{1u}
213 (vs)	210	B_{3u}				292 (s)	294	B_{1u}
223 (s)	225	B_{3u}						
240 (s)	?	B_{3u}						
255 (m)	245	B_{3u}						
283 (s)	288	B_{3u}						

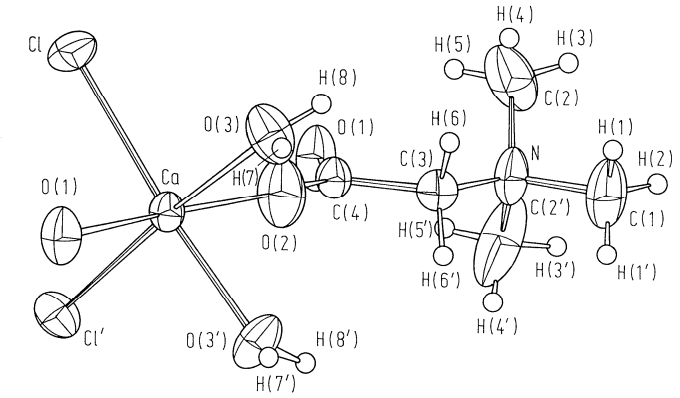

Fig. 66A-1-001. $(CH_3)_3NCH_2COO \cdot CaCl_2 \cdot 2H_2O$ (BCCD). Structure of one formula unit [85Bri2]. Anisotropic temperature parameters are illustrated.

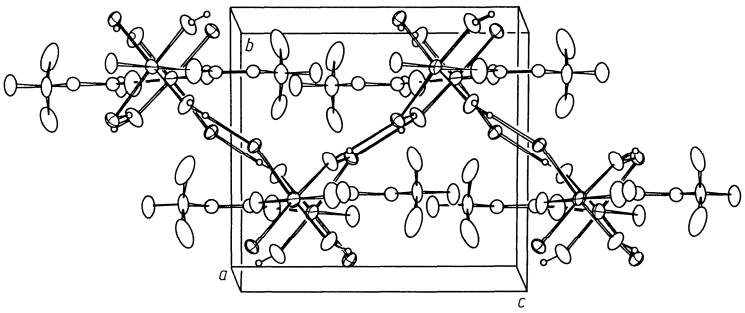

Fig. 66A-1-002. $(CH_3)_3NCH_2COO \cdot CaCl_2 \cdot 2H_2O$ (BCCD). Projection of crystal structure along the *a* axis [85Bri2].

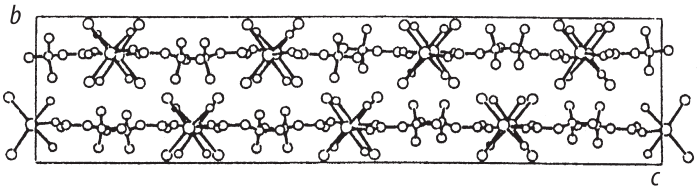

Fig. 66A-1-003. $(CH_3)_3NCH_2COO \cdot CaCl_2 \cdot 2H_2O$ (BCCD). Crystal structure [92Ezp]. T = 90 K. Projection of the four-fold structure along *a*.

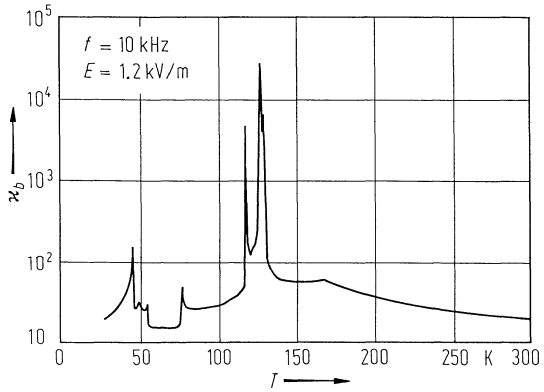

Fig. 66A-1-004. $(CH_3)_3NCH_2COO \cdot CaCl_2 \cdot 2H_2O$ (BCCD). κ_b vs. T [84Rot].

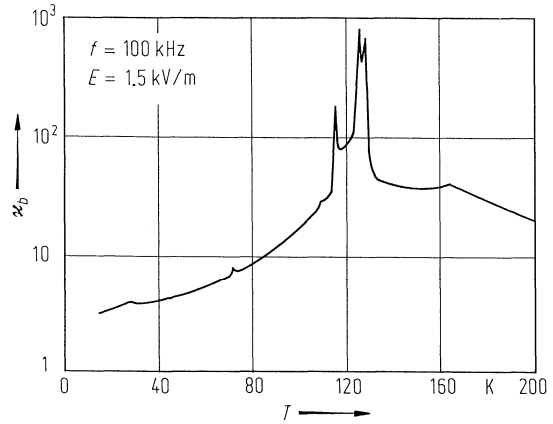

Fig. 66A-1-005. $(CH_3)_3NCD_2COO \cdot CaCl_2 \cdot 2D_2O$. κ_b vs. T [85Klo].

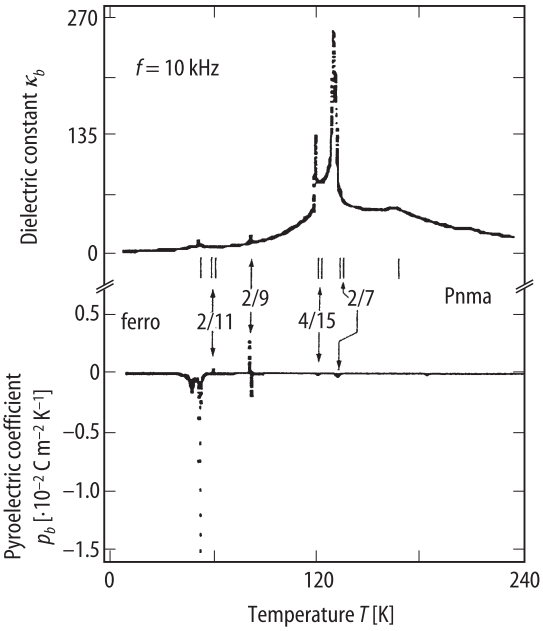

Fig. 66A-1-006. $(CH_3)_3NCH_2COO \cdot CaCl_2 \cdot 2D_2O$. κ_b, p_b vs. T [91Rib1]. p_b: pyroelectric coefficient along b axis. The wave vectors of long-period modulated structures are indicated.

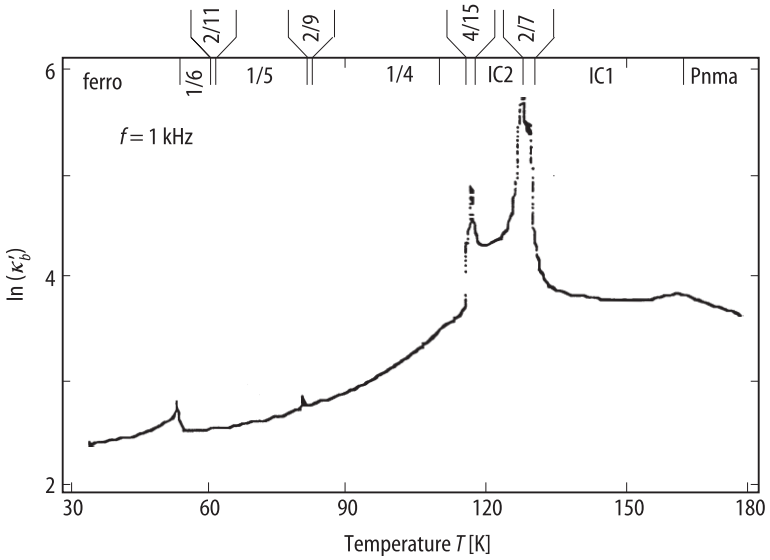

Fig. 66A-1-007. $(CH_3)_3NCH_2COO \cdot CaCl_2 \cdot 2D_2O$. $\ln(\kappa_b')$ vs. T [93Alm]. The wave vectors of long-period modulated structures are denoted at the top of figure. IC: incommensurately modulated phase.

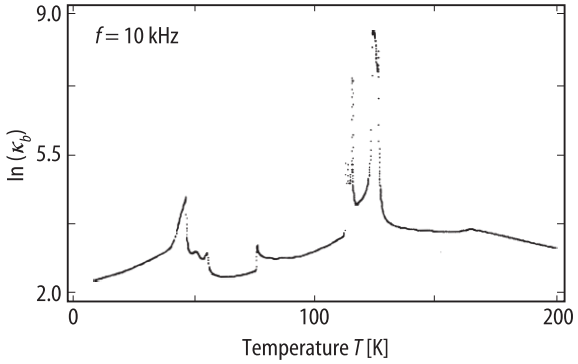

Fig. 66A-1-008. $(CH_3)_3NCH_2COO \cdot CaCl_2 \cdot 2H_2O$ (BCCD). $\ln(\kappa_b)$ vs. T [89Rib1].

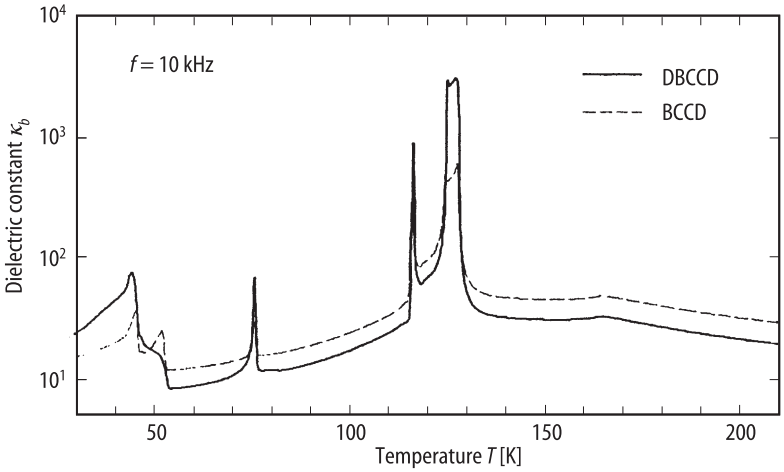

Fig. 66A-1-009. $(CH_3)_3NCH_2COO \cdot CaCl_2 \cdot 2H_2O$ (BCCD), $(CD_3)_3NCD_2COO \cdot CaCl_2 \cdot 2D_2O$ (DBCCD). κ_b vs. T [94Kam].

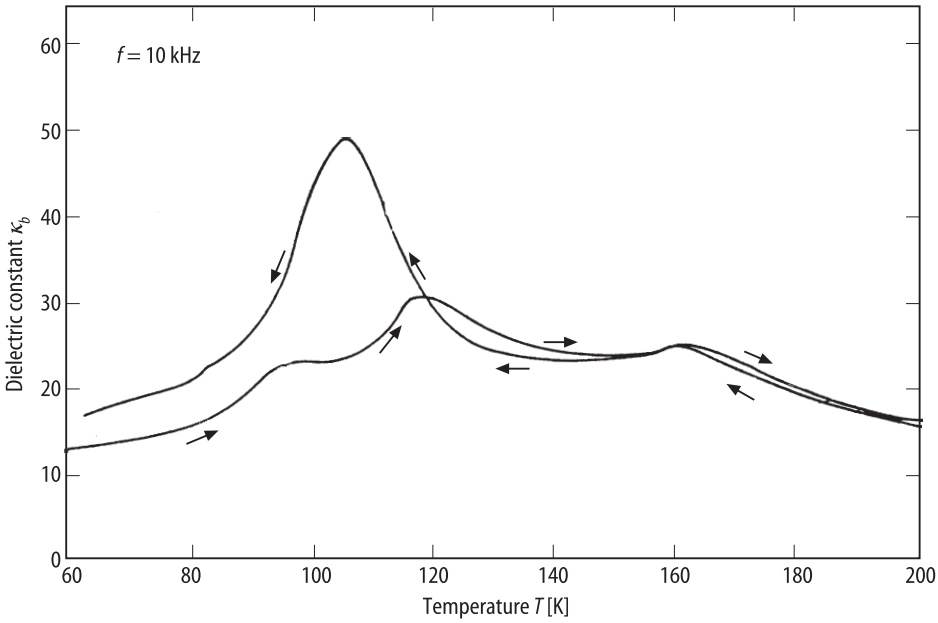

Fig. 66A-1-010. $(CH_3)_3NCH_2COO \cdot CaCl_2 \cdot 2H_2O$ (BCCD). κ_b vs. T [91Met]. Irradiated with ^{60}Co γ-ray with $2 \cdot 10^4$ Gy.

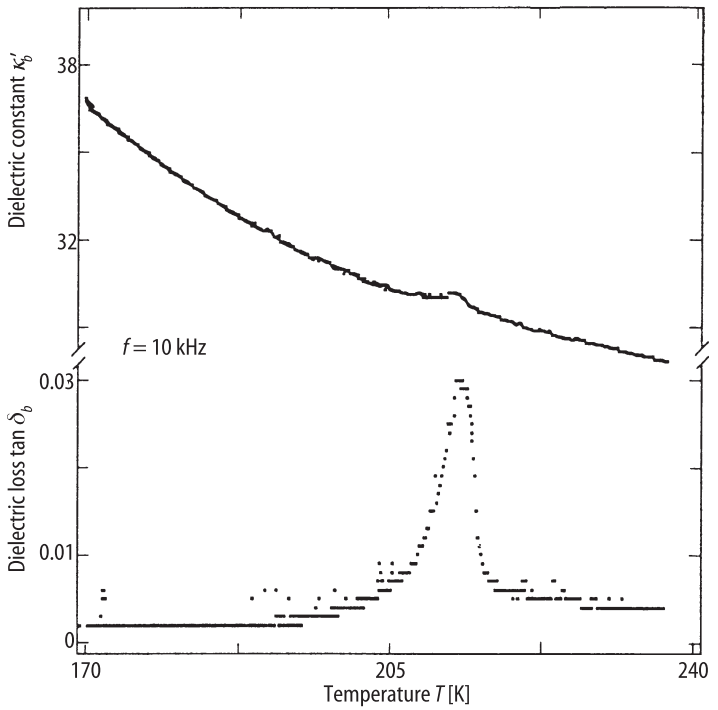

Fig. 66A-1-011. $(CH_3)_3NCH_2COO \cdot CaCl_2 \cdot 2D_2O$. κ_b', tan δ_b vs. T around 218 K anomaly [91Rib1].

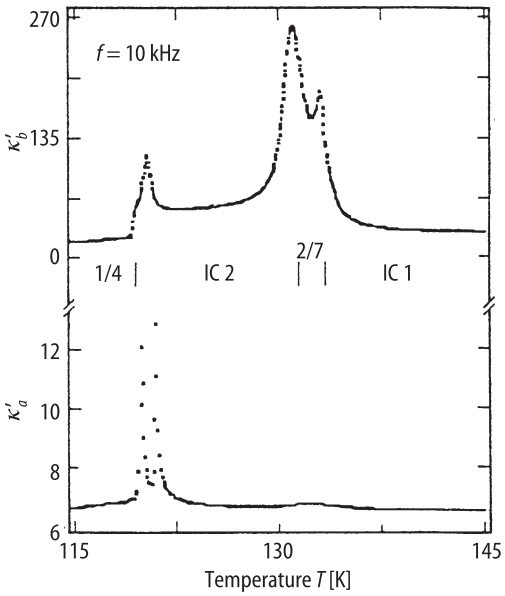

Fig. 66A-1-012. $(CH_3)_3NCH_2COO \cdot CaCl_2 \cdot 2D_2O$. κ'_a, κ'_b vs. T around 130 K [91Rib1]. Wave numbers of modulated structures are indicated. IC: incommensurately modulated phase.

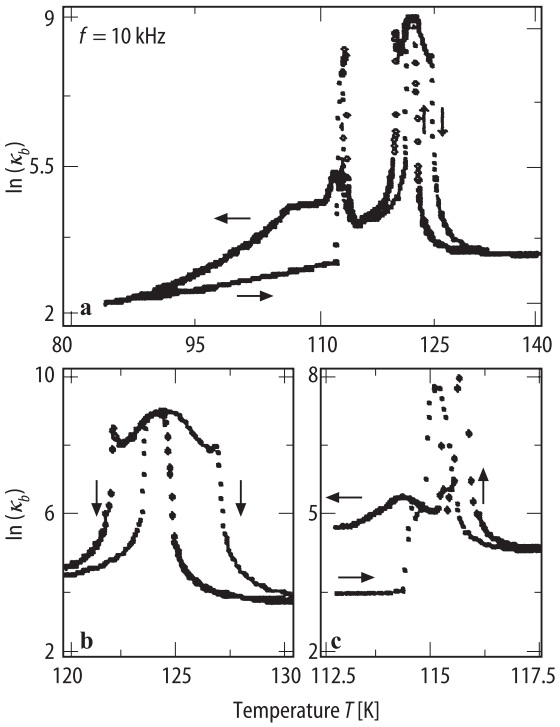

Fig. 66A-1-013. $(CH_3)_3NCH_2COO \cdot CaCl_2 \cdot 2H_2O$ (BCCD). (**a**) $\ln(\kappa_b)$ vs. T [90Rib1]. Details of the anomalies are shown in (**b**) and (**c**).

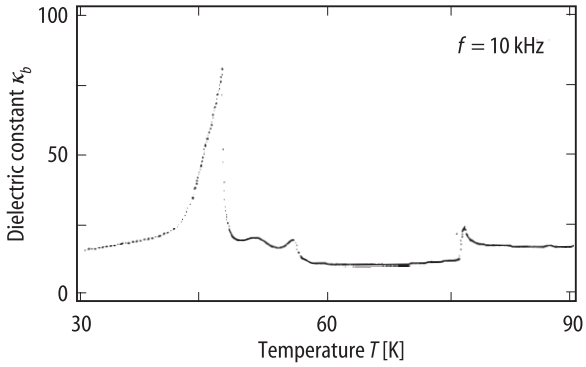

Fig. 66A-1-014. $(CH_3)_3NCH_2COO \cdot CaCl_2 \cdot 2H_2O$ (BCCD). κ_b vs. T in low temperature region [89Rib1].

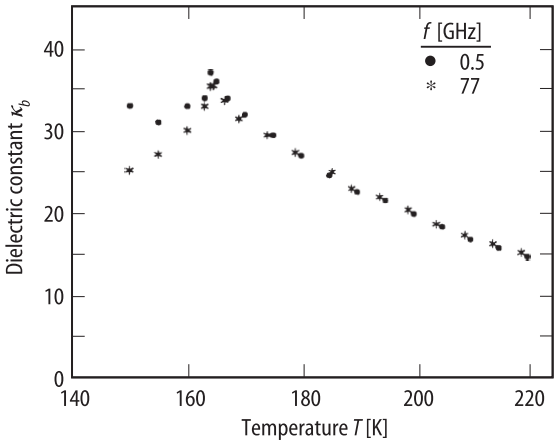

Fig. 66A-1-015. $(CH_3)_3NCH_2COO \cdot CaCl_2 \cdot 2H_2O$ (BCCD). κ_b vs. T in UHF and mm wave region [95Ban]. Parameter: f.

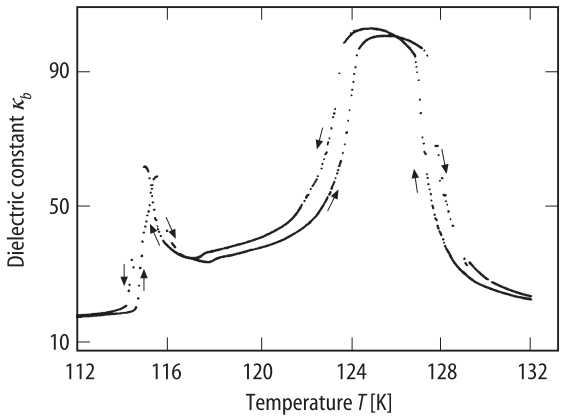

Fig. 66A-1-016. $(CH_3)_3NCH_2COO \cdot CaCl_2 \cdot 2H_2O$ (BCCD). Thermal hysteresis of κ_b vs. T around 120 K [95Sve]. f = 1 kHz. Cooling and heating rate: 0.4 K min^{-1}.

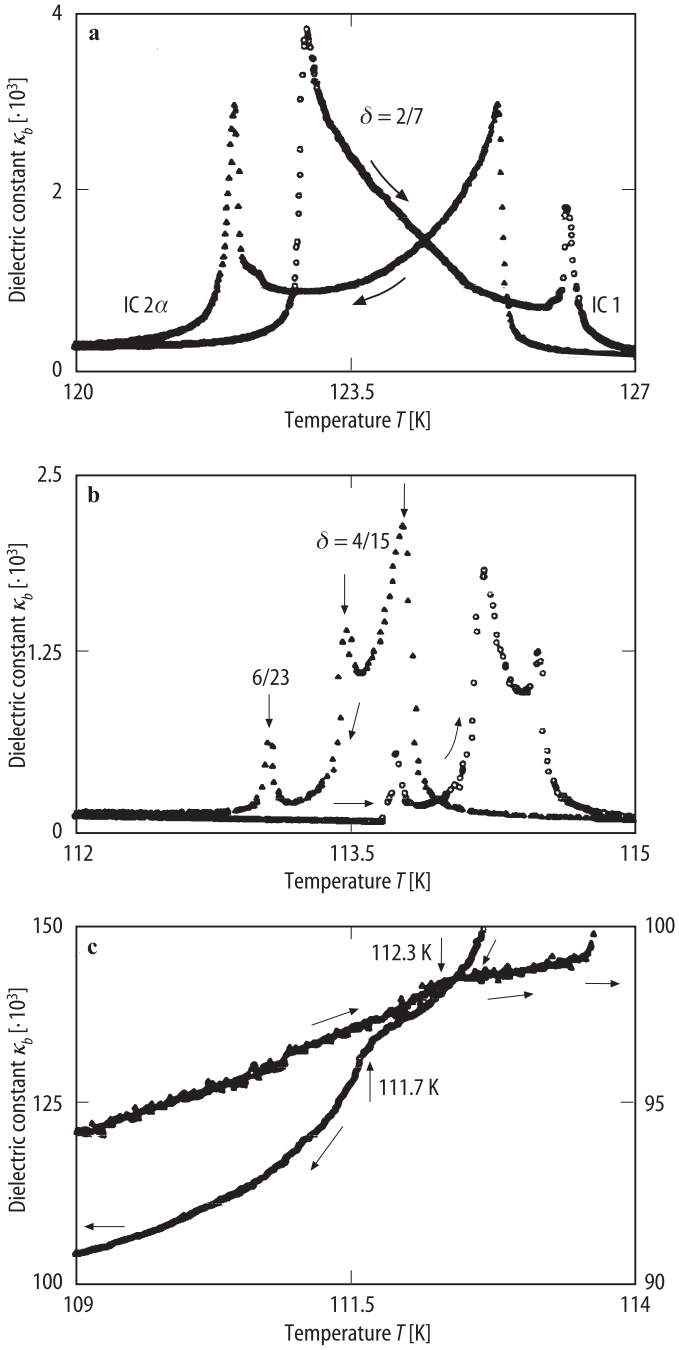

Fig. 66A-1-017. $(CH_3)_3NCH_2COO \cdot CaCl_2 \cdot 2H_2O$ (BCCD). Thermal hysteresis of κ_b vs. T [91Cha]. f = 10 kHz. Cooling and heating rate: 0.1 K min^{-1}. (**a**) 120 K < T < 127 K. (**b**) 112 K < T < 115 K. (**c**) 109 K < T < 114 K. IC: incommensurately modulated phase.

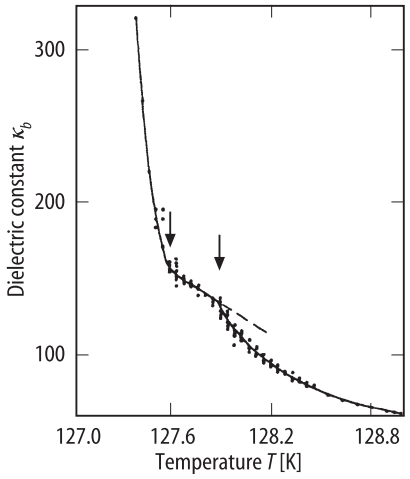

Fig. 66A-1-018. $(CH_3)_3NCH_2COO \cdot CaCl_2 \cdot 2H_2O$ (BCCD). κ_b vs. T around 128 K [95Sve]. f = 1 kHz. Two arrows indicate the range where δ = 5/17 is marked. Cooling run.

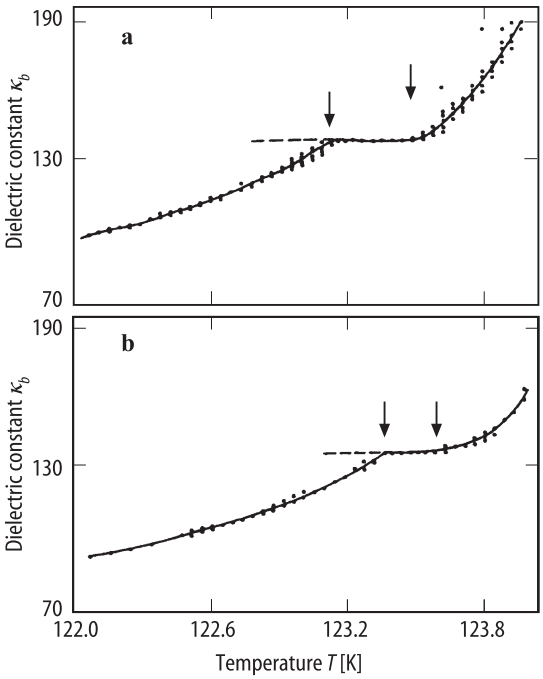

Fig. 66A-1-019. $(CH_3)_3NCH_2COO \cdot CaCl_2 \cdot 2H_2O$ (BCCD). κ_b vs. T around 123 K [95Sve]. Parameter: T_{13}. f = 1 kHz. T_{13}: component of stress tensor. (**a**) T_{13} = 0. (**b**) $T_{13} = 3 \cdot 10^5$ N m^{-2}. Two arrows in each figure indicate the range where δ = 7/25 is observed.

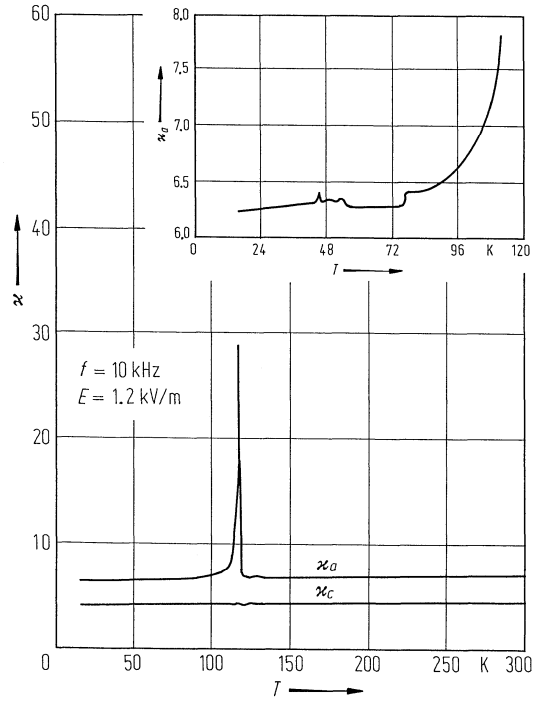

Fig. 66A-1-020. $(CH_3)_3NCH_2COO \cdot CaCl_2 \cdot 2H_2O$ (BCCD). κ_a, κ_c vs. T [84Rot].

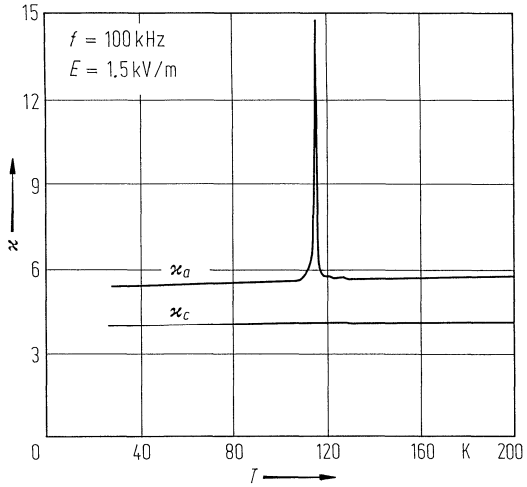

Fig. 66A-1-021. $(CH_3)_3NCD_2COO \cdot CaCl_2 \cdot 2D_2O$. κ_a, κ_c vs. T [85Klo].

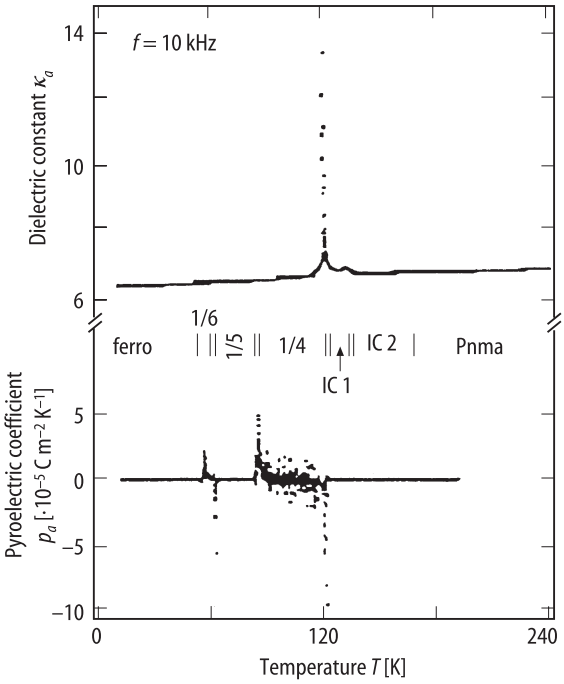

Fig. 66A-1-022. $(CH_3)_3NCH_2COO \cdot CaCl_2 \cdot 2D_2O$. κ_a, p_a vs. T [91Rib1]. p_a: pyroelectric coefficient along a axis.

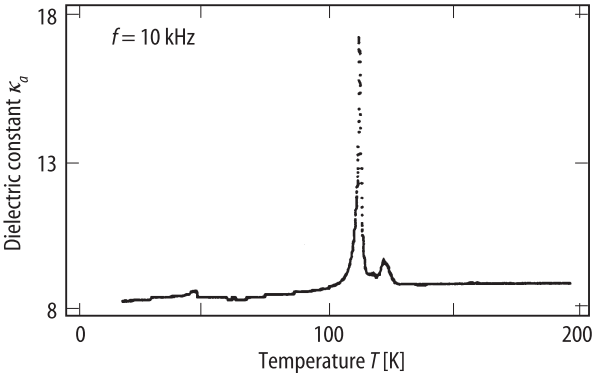

Fig. 66A-1-023. $(CH_3)_3NCH_2COO \cdot CaCl_2 \cdot 2H_2O$ (BCCD). κ_a vs. T [89Rib1].

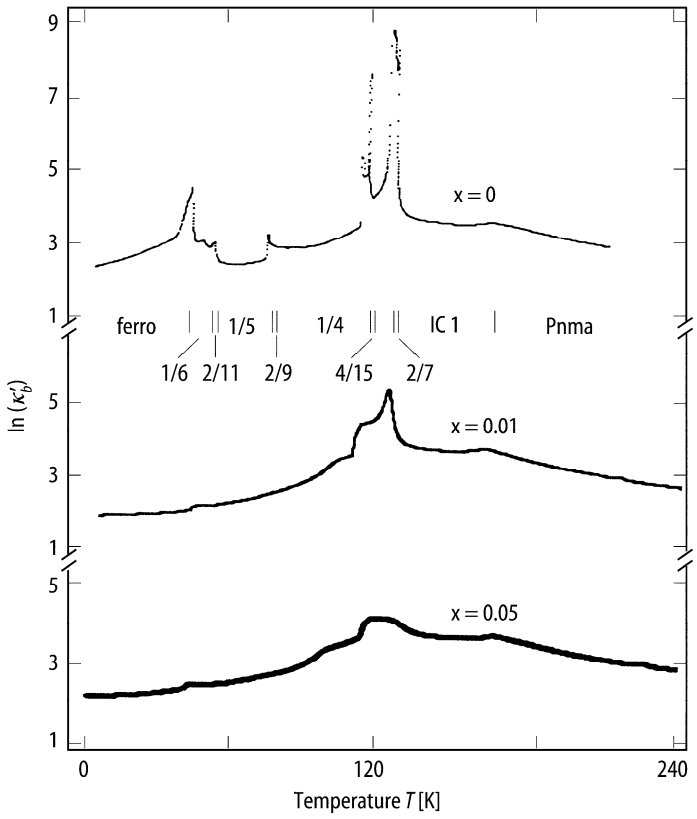

Fig. 66A-1-024. $(CH_3)_3NCH_2COO \cdot (Ca_{1-x}Mn_x)Cl_2 \cdot 2H_2O$. $\ln(\kappa'_b)$ vs. T [91Rib2]. Parameter: x. Wave numbers of modulated structures are indicated. IC: incommensurately modulated structure.

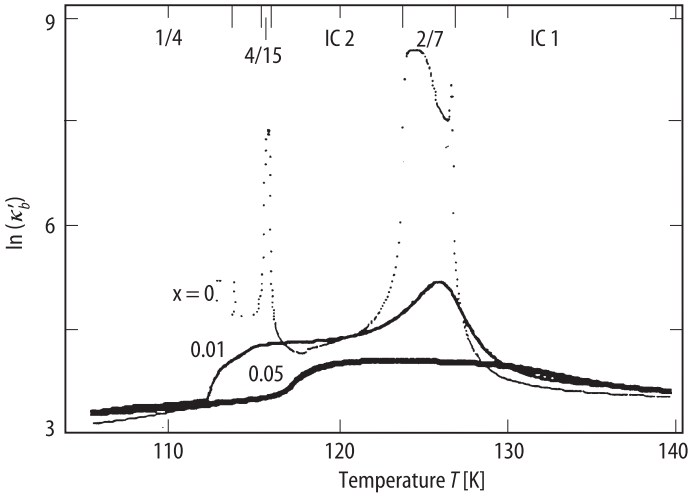

Fig. 66A-1-025. $(CH_3)_3NCH_2COO \cdot (Ca_{1-x}Mn_x)Cl_2 \cdot 2H_2O$. $\ln(\kappa'_b)$ vs. T in the temperature range 100...140 K [91Rib2]. Parameter: x. Wave numbers of modulated structures are denoted at the top of the figure. IC: incommensurately modulated structure.

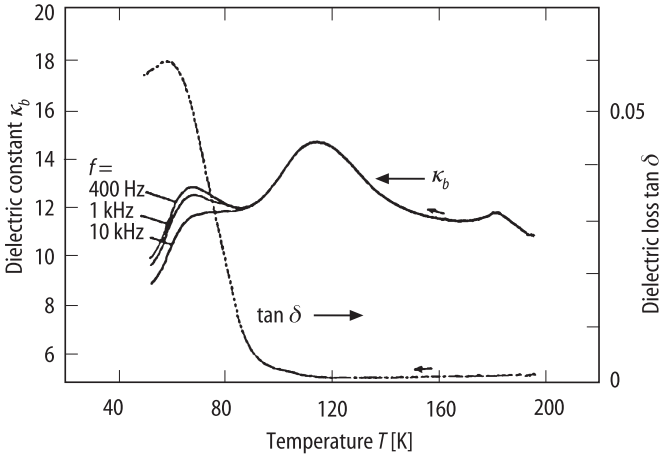

Fig. 66A-1-026. $(CH_3)_3NCH_2COO \cdot (Cl_{0.93}Br_{0.07})Cl_2 \cdot 2H_2O$. κ_b, $\tan\delta$ vs. T at p = 83...129 MPa [92LeM]. Parameter: f.

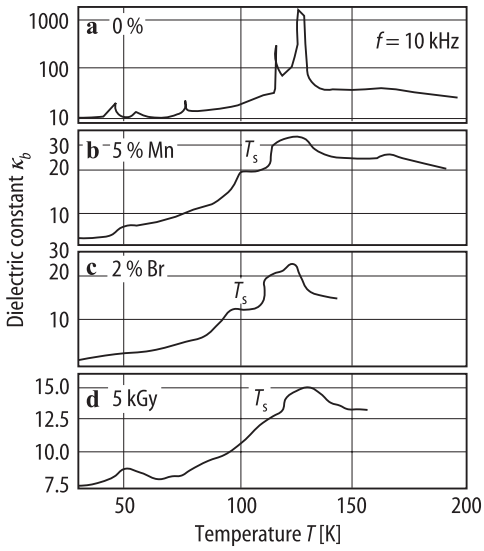

Fig. 66A-1-027. $(CH_3)_3NCH_2COO \cdot CaCl_2 \cdot 2H_2O$ (BCCD). Effect of impurities on κ_b vs. T [94LeM]. (**a**) Pure crystal. (**b**) 5 % Mn doped crystal. (**c**) 2 % Br doped crystal. (**d**) 5 kGy γ-ray irradiated crystal. T_s denotes defect induced anomaly.

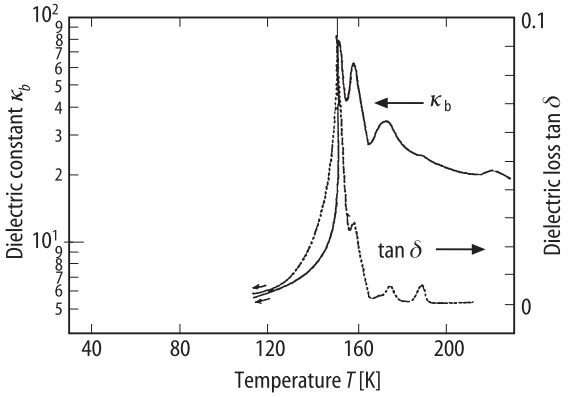

Fig. 66A-1-028. $(CH_3)_3NCH_2COO \cdot Ca(Cl_{0.98}Br_{0.02})_2 \cdot 2H_2O$. κ_b, tan δ vs. T at p = 316…345 MPa [92LeM].

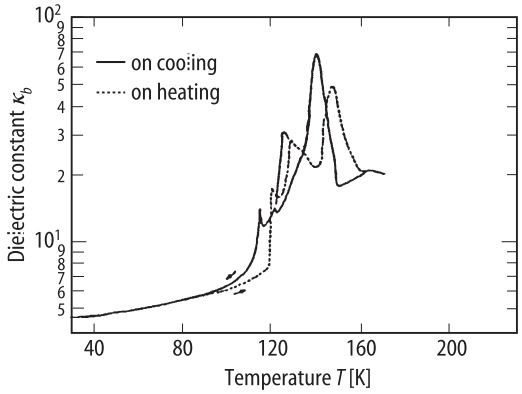

Fig. 66A-1-029. $(CH_3)_3NCH_2COO \cdot Ca(Cl_{0.98}Br_{0.02})_2 \cdot 2H_2O$. κ_b vs. T at p = 174…243 MPa [92LeM].

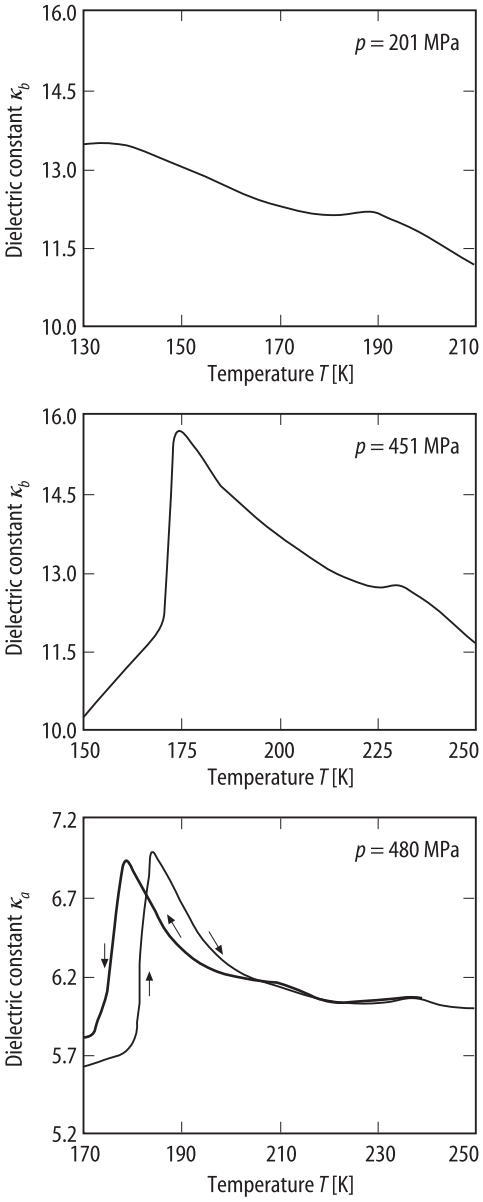

Fig. 66A-1-030. $(CH_3)_3NCH_2COO \cdot Ca(Cl_{0.936}Br_{0.064})_2 \cdot 2H_2O$. κ_a, κ_b vs. T at various p [90AoR].

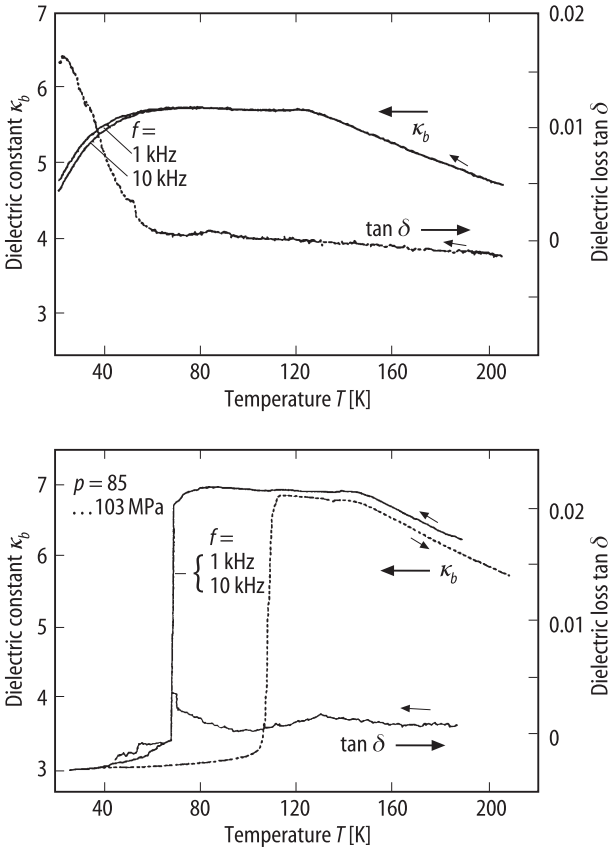

Fig. 66A-1-031. $(CH_3)_3NCH_2COO \cdot Ca(Cl_{0.8}Br_{0.2})_2 \cdot 2H_2O$. κ_b, tan δ vs. T at p = 0 MPa and 85…103 MPa [92LeM].

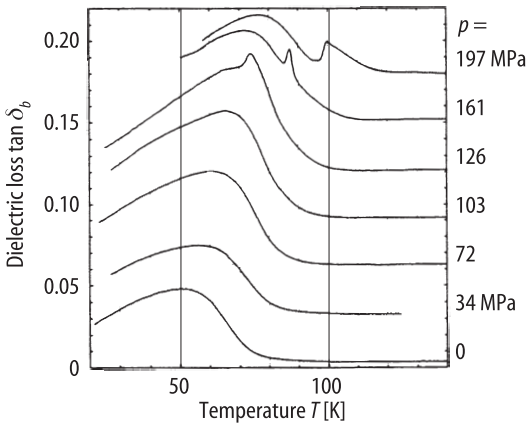

Fig. 66A-1-032. $(CH_3)_3NCH_2COO \cdot CaCl_2 \cdot 2H_2O$ doped with 7 % Br. tan δ_b vs. T [94LeM]. Parameter: p.

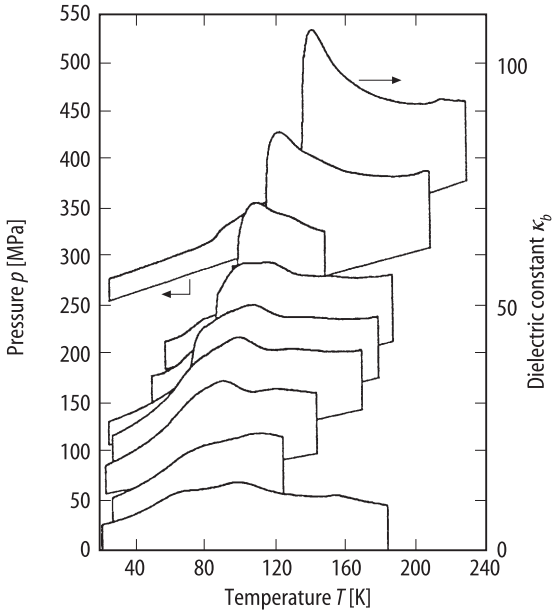

Fig. 66A-1-033. $(CH_3)_3NCH_2COO \cdot Ca(Cl_{0.93}Br_{0.07})_2 \cdot 2H_2O$. κ_b vs. T at various p [92LeM].

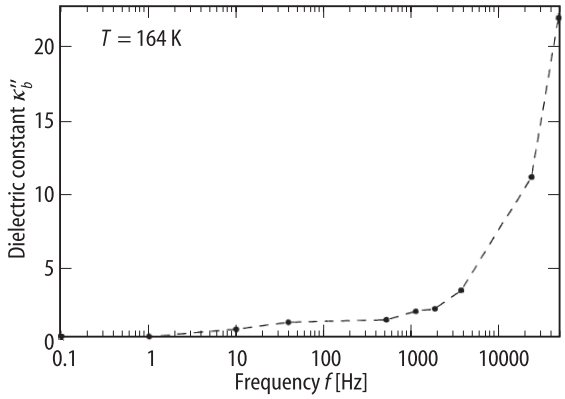

Fig. 66A-1-034. $(CH_3)_3NCH_2COO \cdot CaCl_2 \cdot 2H_2O$ (BCCD). κ_b'' vs. f [95Ban]. T = 164 K.

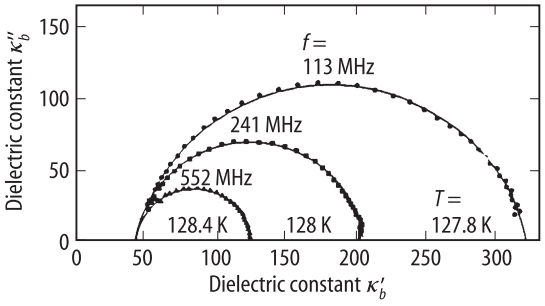

Fig. 66A-1-035. $(CH_3)_3NCH_2COO \cdot CaCl_2 \cdot 2H_2O$ (BCCD). κ_b' vs. κ_b'' [90Fre]. Parameter: T.

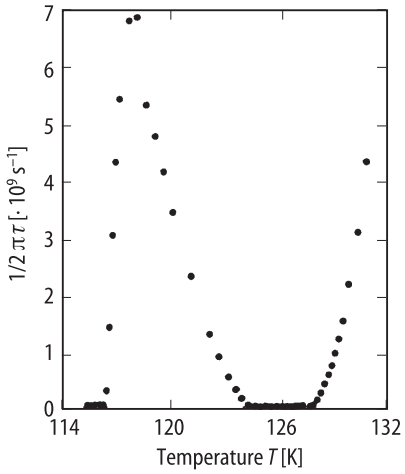

Fig. 66A-1-036. $(CH_3)_3NCH_2COO \cdot CaCl_2 \cdot 2H_2O$ (BCCD). $1/2\pi\tau$ vs. T [90Fre]. τ: dielectric relaxation time.

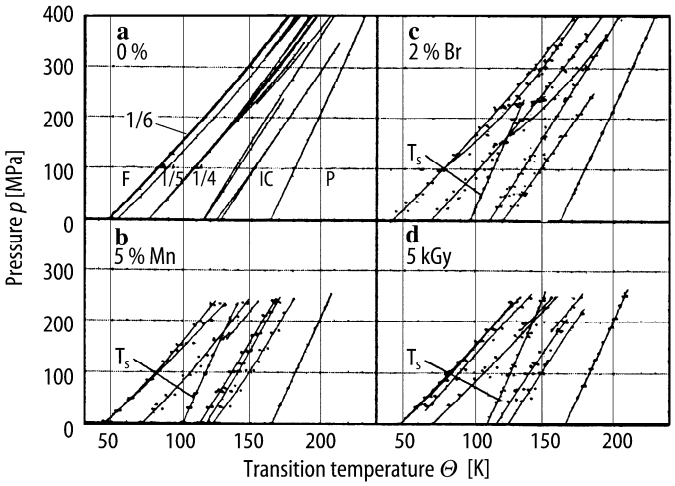

Fig. 66A-1-037. $(CH_3)_3NCH_2COO \cdot CaCl_2 \cdot 2H_2O$ (BCCD). $p - \Theta$ phase diagram for doped and γ-ray irradiated crystals [94LeM]. (**a**) Pure crystal. (**b**) 5 % Mn doped crystal. (**c**) 2 % Br doped crystal. (**d**) 5 kGy γ-ray irradiated crystal. T_s: line of defect induced anomaly. P: paraelectric region. F: ferroelectric region. IC: incommensurately modulated phase. Fractions indicate lattice modulation wave vectors in the units of c^*.

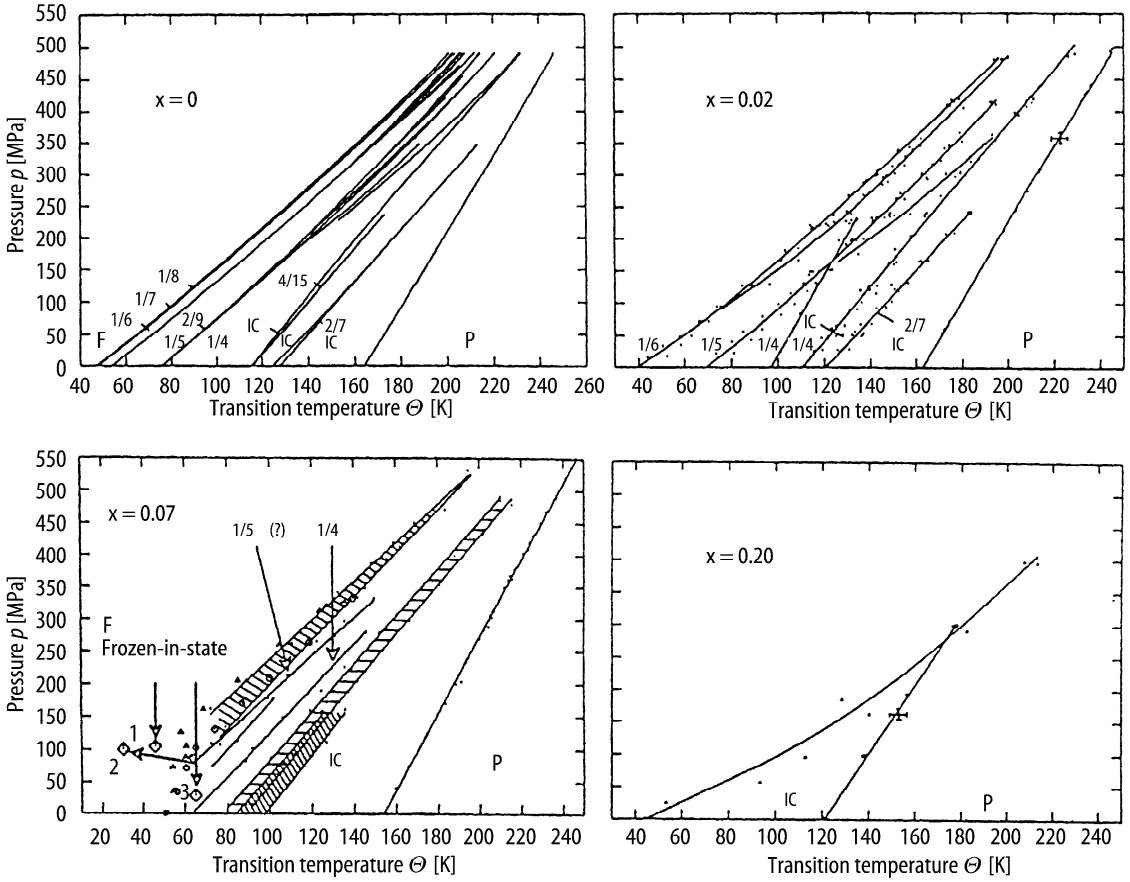

Fig. 66A-1-038. $(CH_3)_3NCH_2COO \cdot Ca(Cl_{1-x}Br_x)_2 \cdot 2H_2O$. $p - \Theta$ phase diagram for various x [92LeM]. P: paraelectric region. F: ferroelectric region. IC: incommensurately modulated phase. Fractions indicate the wave numbers in the units of c^* of structure modulation in the commensurately modulated phase. Hatched regions indicate thermal hysteresis.

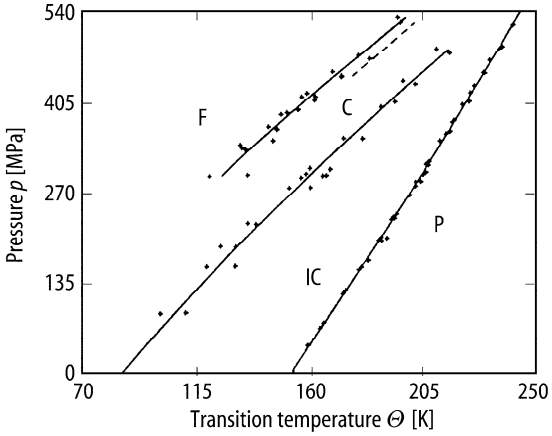

Fig. 66A-1-039. $(CH_3)_3NCH_2COO \cdot Ca(Cl_{0.936}Br_{0.064})_2 \cdot 2H_2O$. $p - \Theta$ phase diagram [90AoR]. P: paraelectric region. F: ferroelectric region. IC: incommensurately modulated phase. C: commensurately modulated phase.

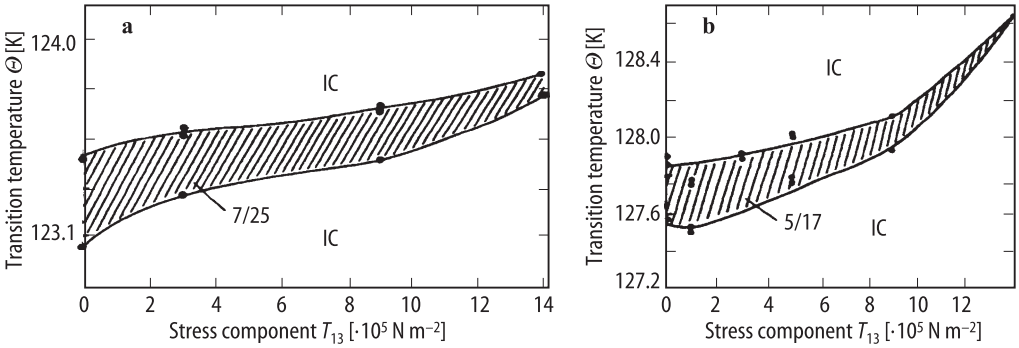

Fig. 66A-1-040. $(CH_3)_3NCH_2COO \cdot CaCl_2 \cdot 2H_2O$ (BCCD). $\Theta - T_{13}$ phase diagram [95Sve]. T_{13}: stress component. (**a**) Region of $\delta = 7/25$ phase. (**b**) Region of $\delta = 5/17$ phase. IC: incommensurately modulated phase.

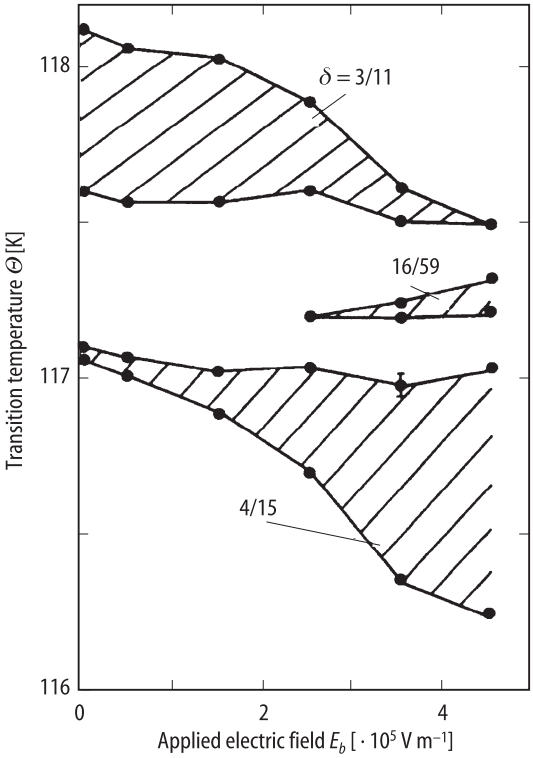

Fig. 66A-1-041. $(CH_3)_3NCH_2COO \cdot CaCl_2 \cdot 2H_2O$ (BCCD). $\Theta - E_b$ phase diagram [95Sve]. E_b: applied electric field in *b* direction.

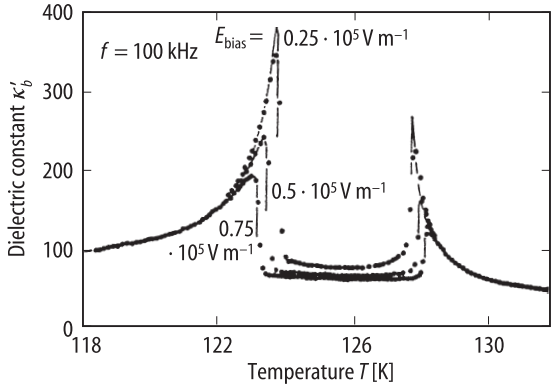

Fig. 66A-1-042. $(CH_3)_3NCH_2COO \cdot CaCl_2 \cdot 2H_2O$ (BCCD). κ'_b vs. T [90Fre]. Parameter: E_{bias}.

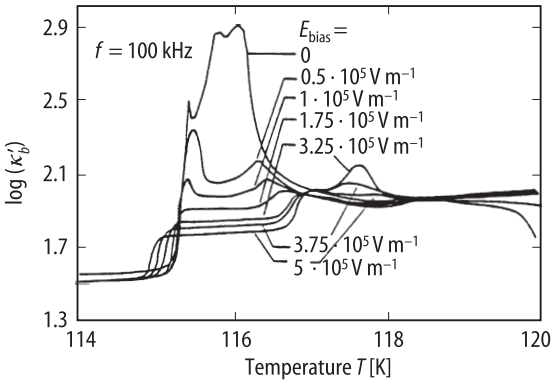

Fig. 66A-1-043. $(CH_3)_3NCH_2COO \cdot CaCl_2 \cdot 2H_2O$ (BCCD). $\log(\kappa'_b)$ vs. T [90Fre]. Parameter: E_{bias}.

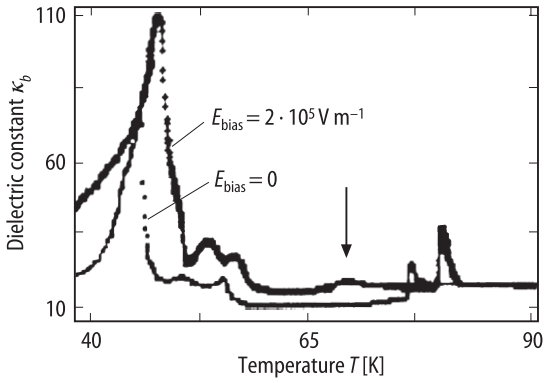

Fig. 66A-1-044. $(CH_3)_3NCH_2COO \cdot CaCl_2 \cdot 2H_2O$ (BCCD). κ_b vs. T [90Rib2]. Parameter: E_{bias}.

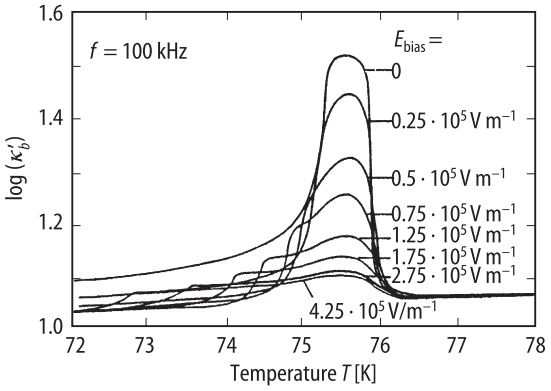

Fig. 66A-1-045. $(CH_3)_3NCH_2COO \cdot CaCl_2 \cdot 2H_2O$ (BCCD). $\log(\kappa_b')$ vs. T [90Fre]. Parameter: E_{bias}.

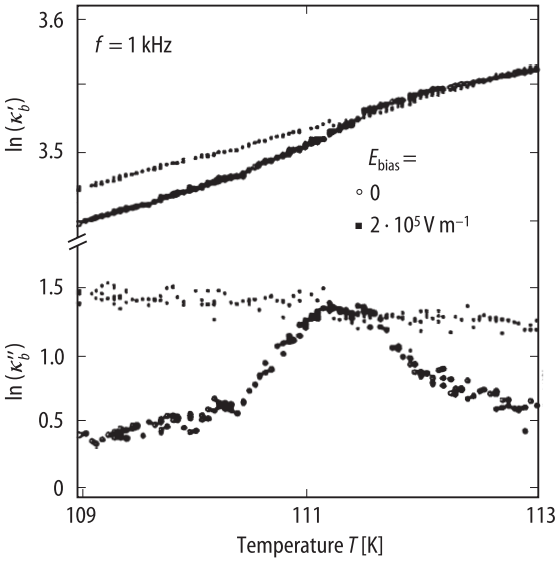

Fig. 66A-1-046. $(CH_3)_3NCH_2COO \cdot CaCl_2 \cdot 2D_2O$. $\ln(\kappa_b')$, $\ln(\kappa_b'')$ vs. T in the vicinity of 111 K anomaly [93Alm]. Parameter: E_{bias}.

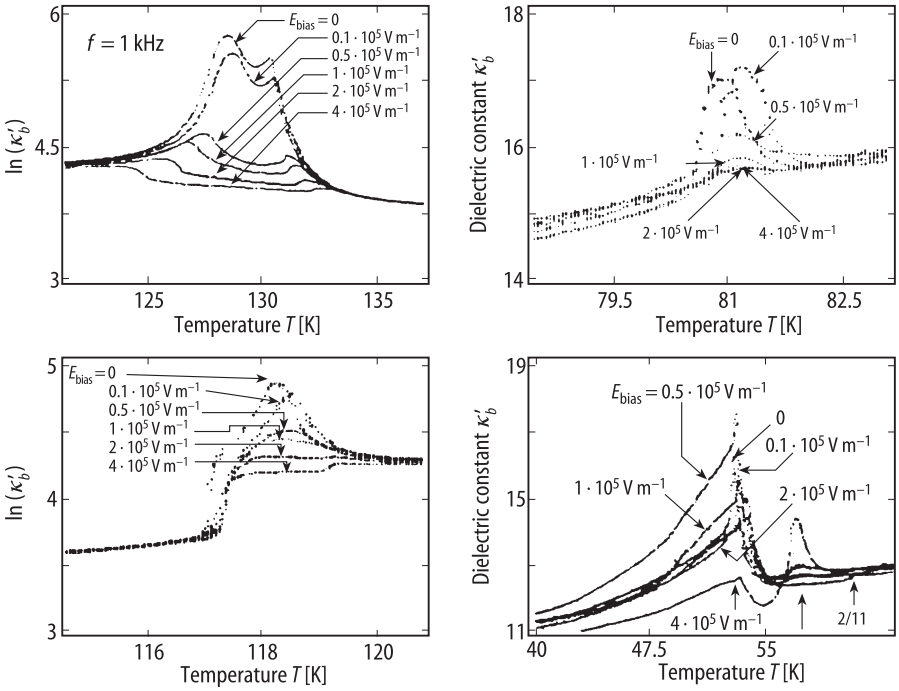

Fig. 66A-1-047. $(CH_3)_3NCH_2COO \cdot CaCl_2 \cdot 2D_2O$. $\ln(\kappa'_b)$, κ'_b vs. T [93Alm]. Parameter: E_{bias}.

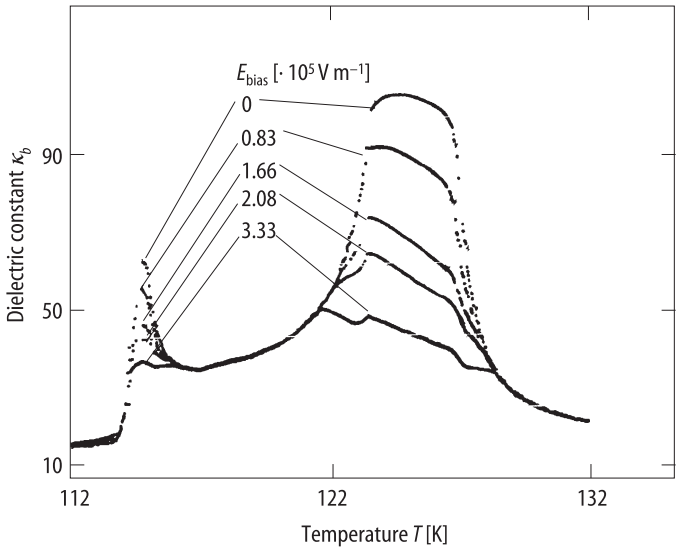

Fig. 66A-1-048. $(CH_3)_3NCH_2COO \cdot CaCl_2 \cdot 2H_2O$ (BCCD). κ_b vs. T [95Sve]. Parameter: E_{bias}. f = 1 kHz.

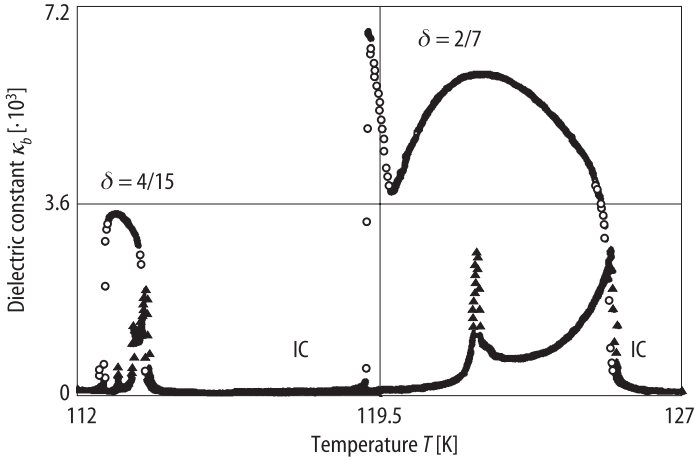

Fig. 66A-1-049. $(CH_3)_3NCH_2COO \cdot CaCl_2 \cdot 2H_2O$ (BCCD). κ_b vs. T [91Cha]. Parameter: applied ac signal field, E_{ac}. f = 10 kHz. Full upside triangle: E_{ac} = 0.01 V m^{-1}. Open circle: E_{ac} = 0.2 V m^{-1}. IC: incommensurately modulated phase.

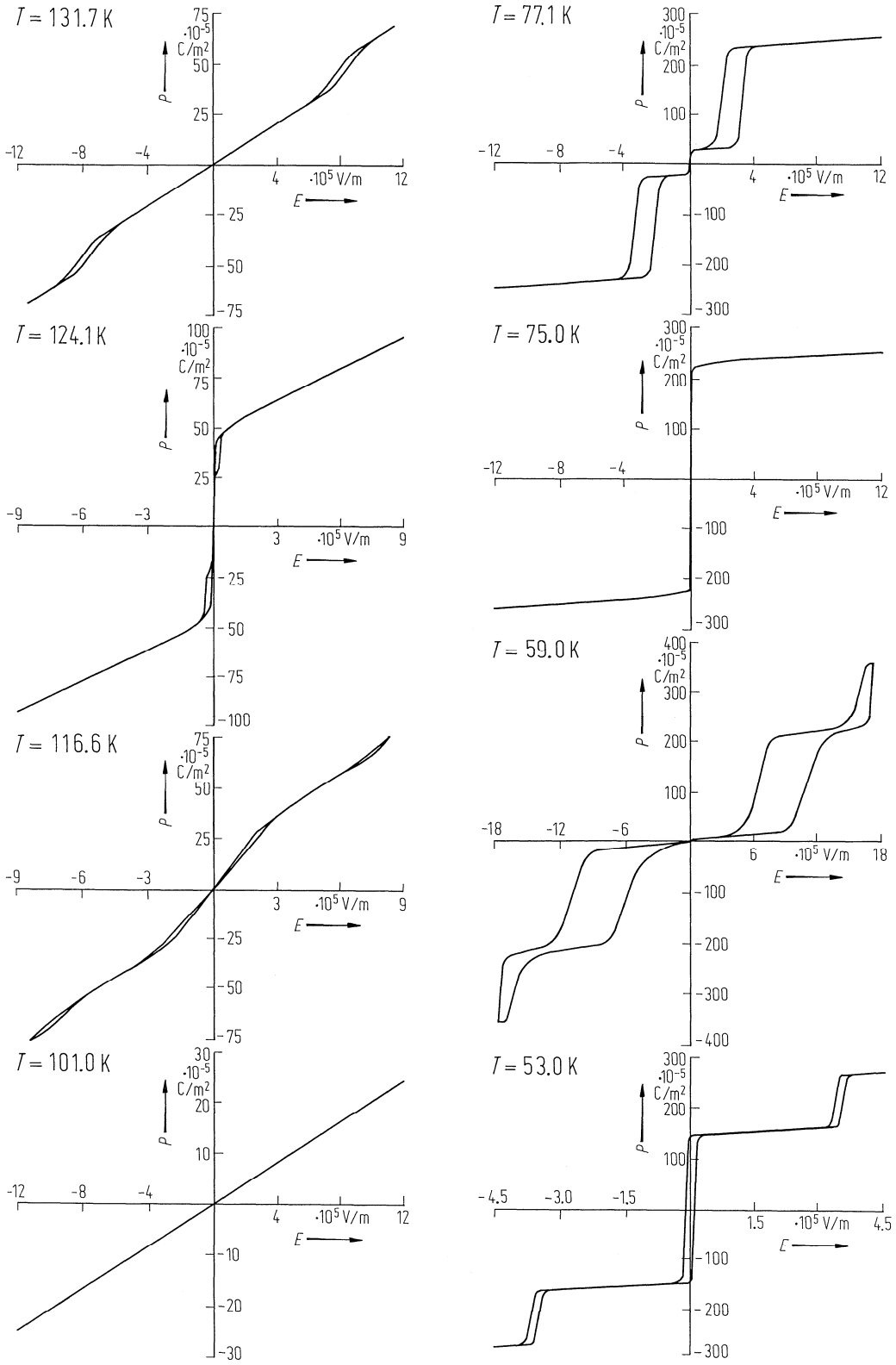

Fig. 66A-1-050. Continued.

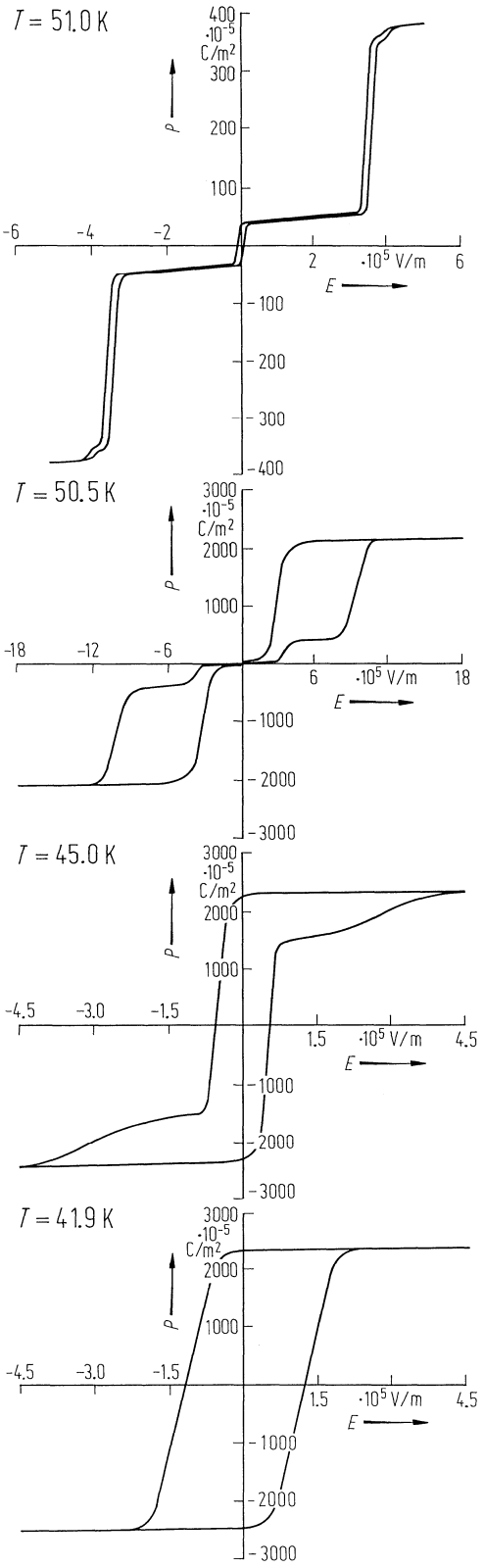

Fig. 66A-1-050. $(CH_3)_3NCH_2COO \cdot CaCl_2 \cdot 2H_2O$ (BCCD). *P* vs. *E* at various *T* [84Rot]. *f* = 1 Hz.

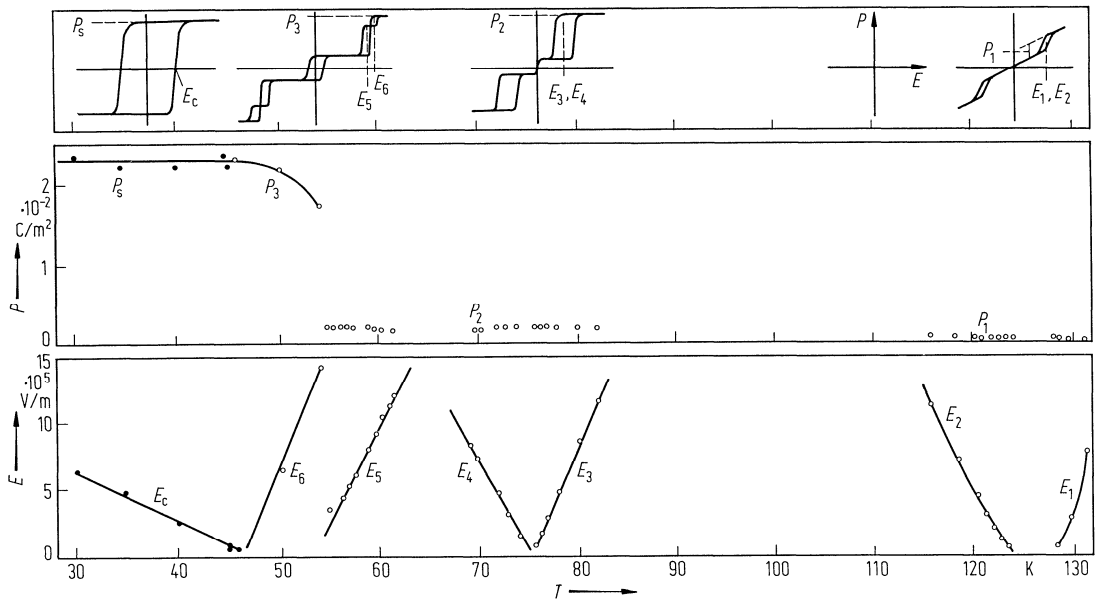

Fig. 66A-1-051. $(CH_3)_3NCH_2COO \cdot CaCl_2 \cdot 2H_2O$ (BCCD). P_s, E_c, P_i, E_i vs. T [85Klo]. Definitions of P_i (i = 1, 2, 3) and E_i (i = 1, ..., 6) are shown in the top figure.

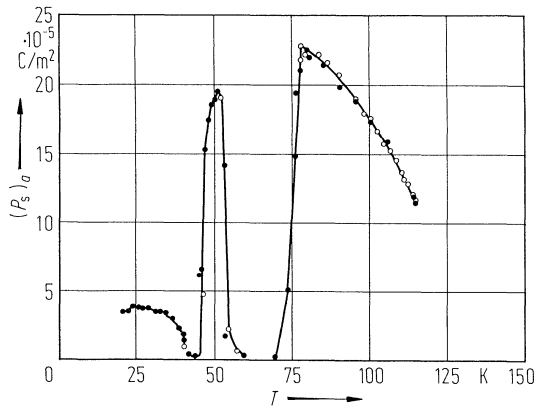

Fig. 66A-1-052. $(CH_3)_3NCH_2COO \cdot CaCl_2 \cdot 2H_2O$ (BCCD). $(P_s)_a$ vs. T [85Klo]. $(P_s)_a$: spontaneous polarization along the *a* axis. f = 1 Hz. Open circle and full circle are data from two different samples.

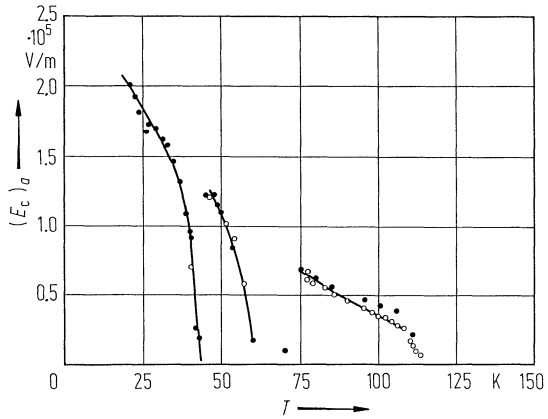

Fig. 66A-1-053. $(CH_3)_3NCH_2COO \cdot CaCl_2 \cdot 2H_2O$ (BCCD). $(E_c)_a$ vs. T [85Klo]. $(E_c)_a$: coercive field along the a axis. f = 1 Hz. Open circle and full circle are data from two different samples.

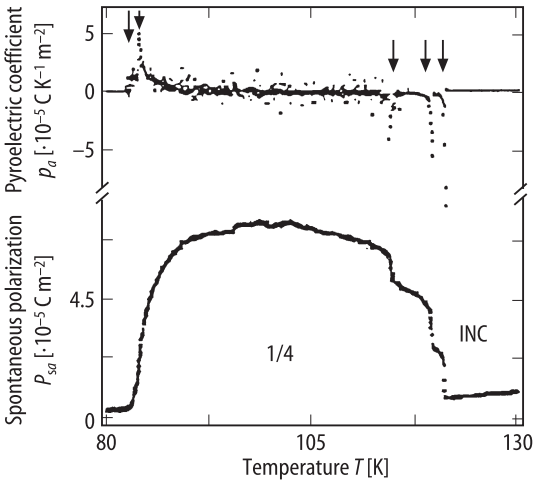

Fig. 66A-1-054. $(CH_3)_3NCH_2COO \cdot CaCl_2 \cdot 2D_2O$. p_a, P_{sa} vs. T around 105 K [91Rib1]. p_a: pyroelectric coefficient along a axis. P_{sa}: spontaneous polarization along a axis. INC: incommensurately modulated phase. Arrows: anomalies in pyroelectric coefficient. Doublet-like arrows correspond to the difference in the local stress by inhomogeneous deuteration.

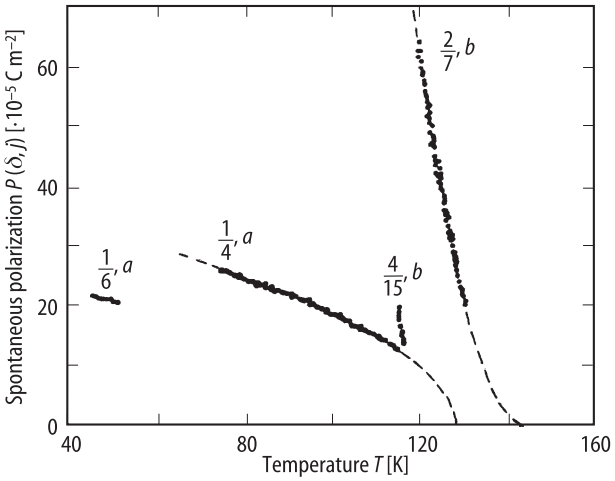

Fig. 66A-1-055. $(CH_3)_3NCH_2COO \cdot CaCl_2 \cdot 2H_2O$ (BCCD). $P(\delta, j)$ vs. T [91Wil]. $P(\delta, j)$: spontaneous polarization of various commensurate phases with modulation wave vector δ in units of c^* and direction of polarization j.

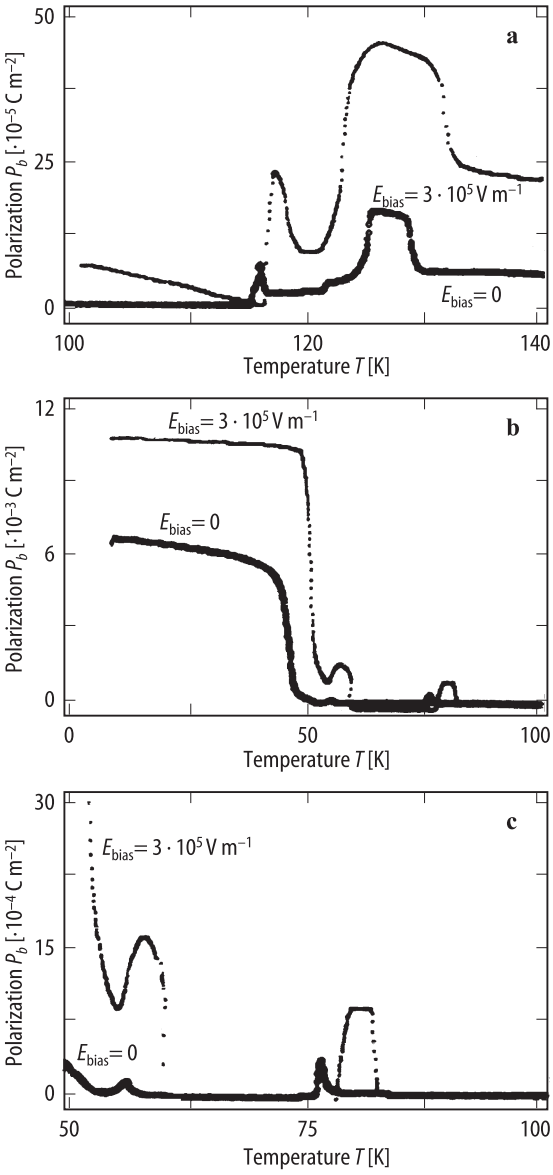

Fig. 66A-1-056. $(CH_3)_3NCH_2COO \cdot CaCl_2 \cdot 2H_2O$ (BCCD). P_b vs. T [89Rib2]. Parameter: E_{bias}. P_b: polarization along the b axis. (**a**) 100 K < T < 140 K. (**b**) 10 K < T < 100 K. (**c**) 50 K < T < 100 K.

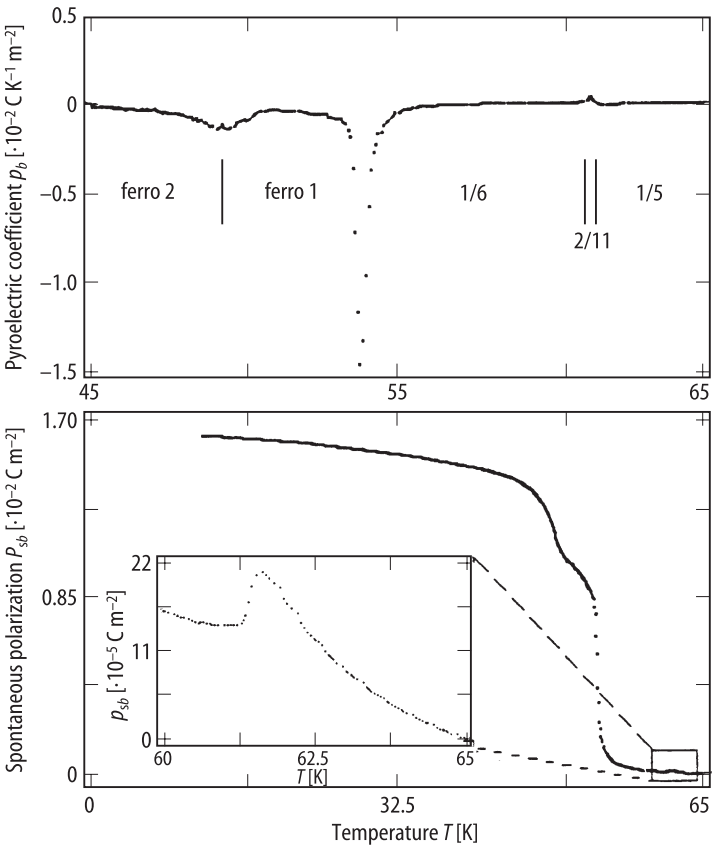

Fig. 66A-1-057. $(CH_3)_3NCH_2COO \cdot CaCl_2 \cdot 2D_2O$. p_b, P_{sb} vs. T in low-temperature region [91Rib1]. p_b: pyroelectric coefficient along b axis. P_{sb}: spontaneous polarization along b axis.

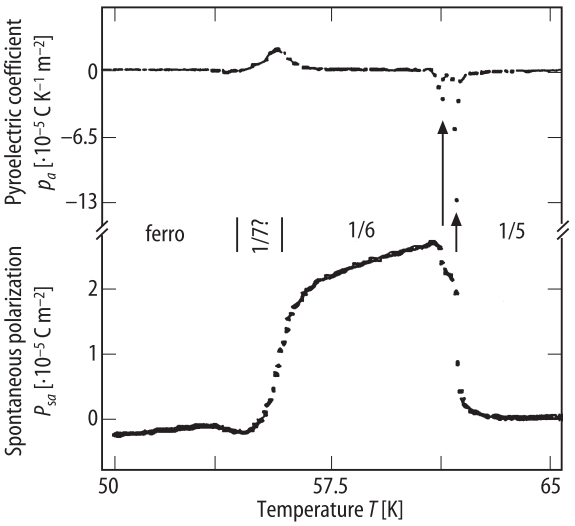

Fig. 66A-1-058. $(CH_3)_3NCH_2COO \cdot CaCl_2 \cdot 2D_2O$. p_a, P_{sa} vs. T around 57.5 K [91Rib1]. p_a: pyroelectric coefficient along a axis. P_{sa}: spontaneous polarization along a axis. Arrows: clear minima in the pyroelectric coefficient.

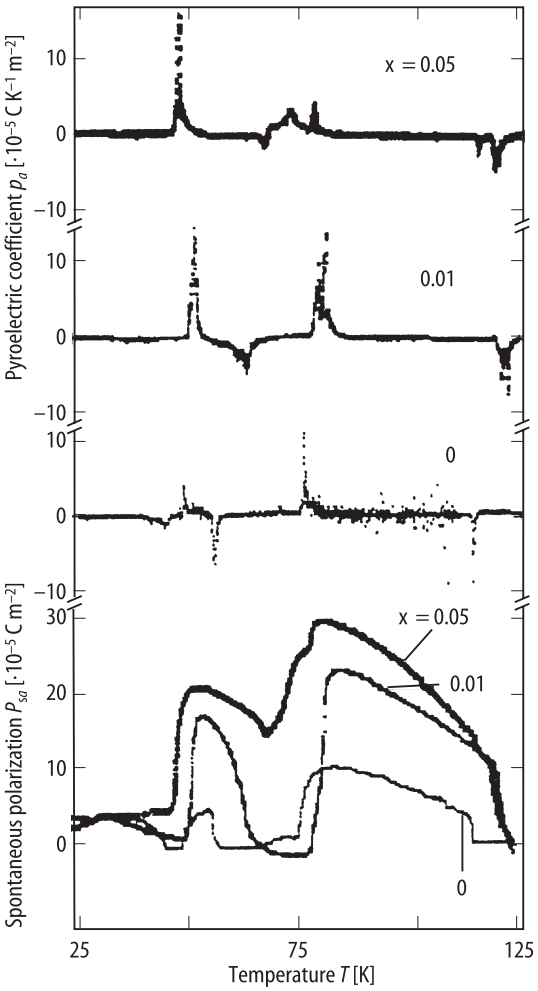

Fig. 66A-1-059. $(CH_3)_3NCH_2COO \cdot (Ca_{1-x}Mn_x)Cl_2 \cdot 2H_2O$. p_a, P_{sa} vs. T [91Rib2]. Parameter: x. p_a: pyroelectric coefficient along a axis. P_{sa}: spontaneous polarization along a axis.

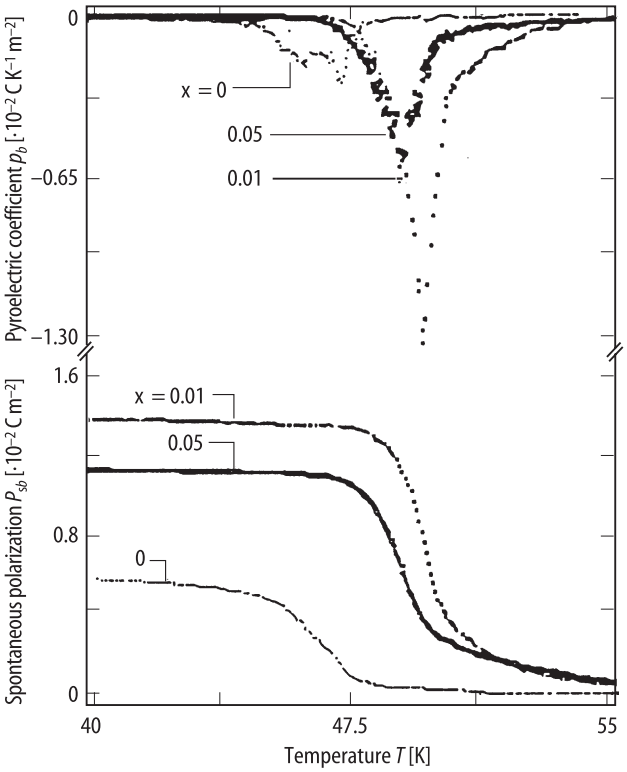

Fig. 66A-1-060. $(CH_3)_3NCH_2COO \cdot (Ca_{1-x}Mn_x)Cl_2 \cdot 2H_2O$. p_b, P_{sb} vs. T in low-temperature region [91Rib2]. Parameter: x. p_b: pyroelectric coefficient along b axis. P_{sb}: spontaneous polarization along b axis.

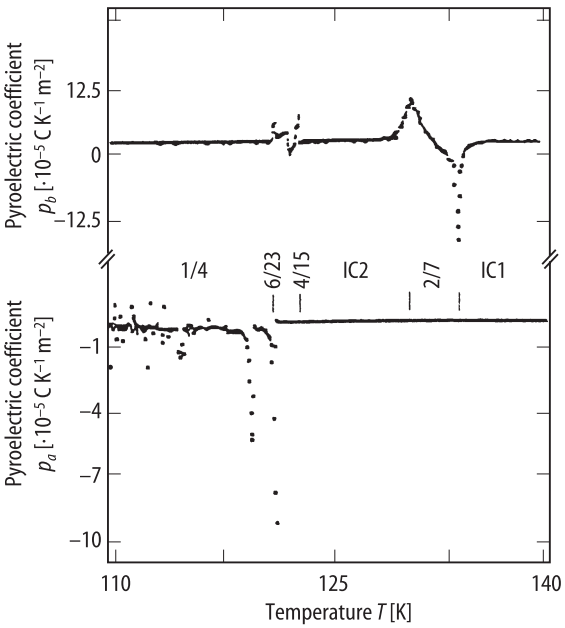

Fig. 66A-1-061. $(CH_3)_3NCH_2COO \cdot CaCl_2 \cdot 2D_2O$. p_a, p_b vs. T around 130 K [91Rib1]. p_a, p_b: pyroelectric coefficient along a and b axes.

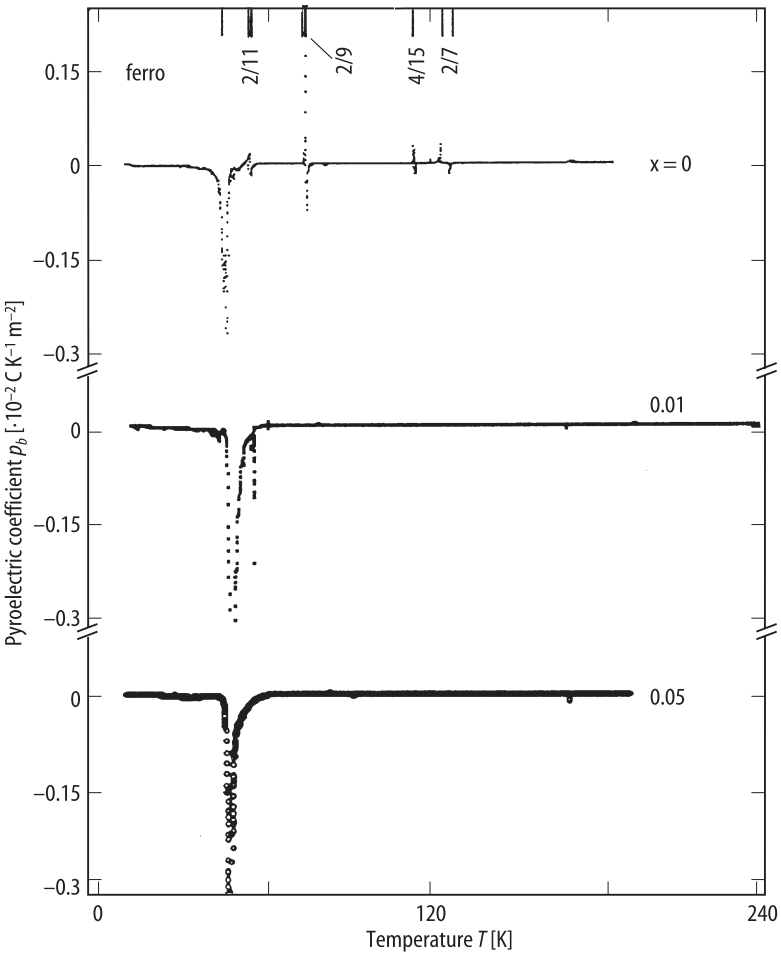

Fig. 66A-1-062. $(CH_3)_3NCH_2COO \cdot (Ca_{1-x}Mn_x)Cl_2 \cdot 2H_2O$. p_b vs. T [91Rib2]. Parameter: x. p_b: pyroelectric coefficient along b axis.

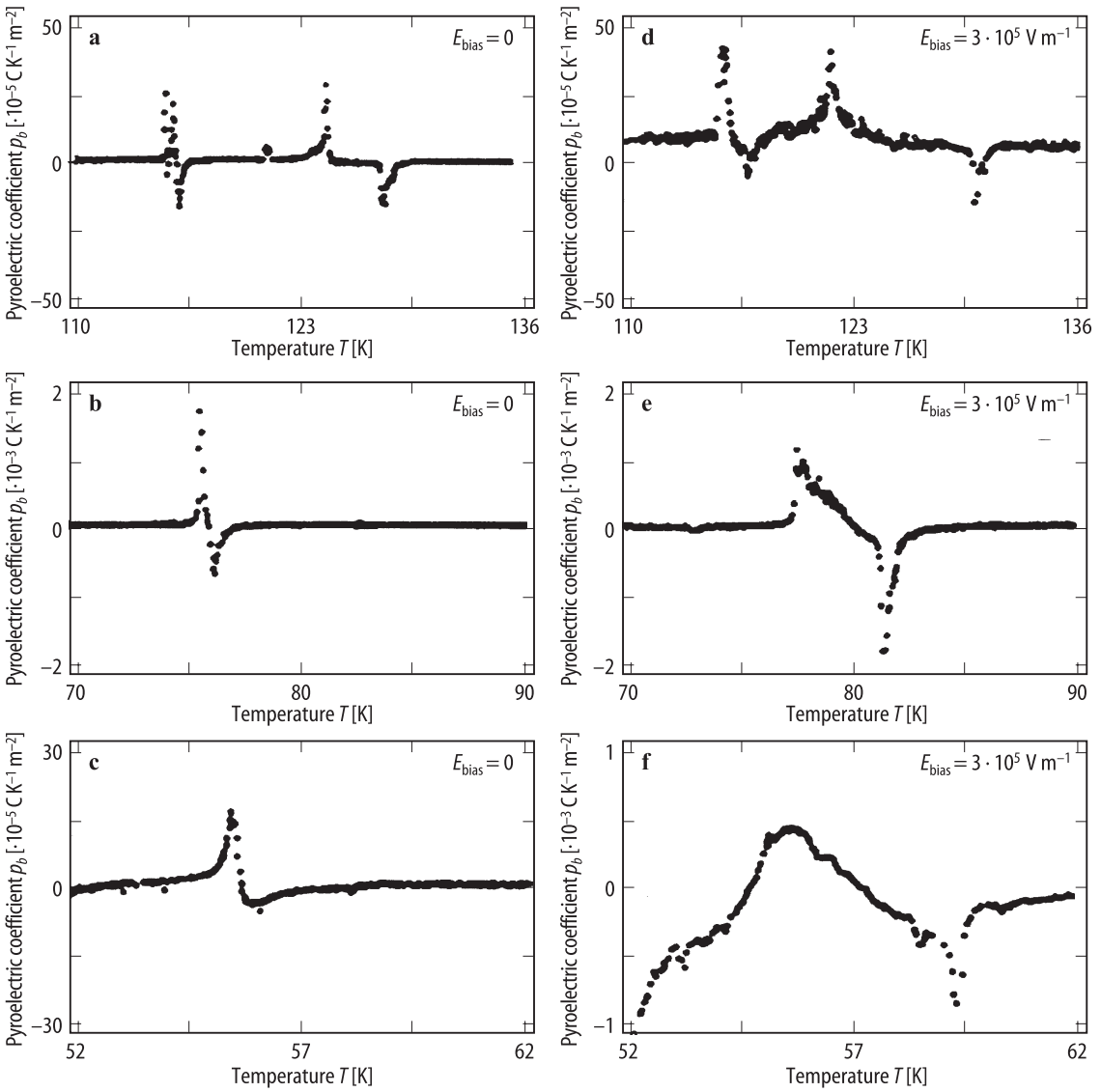

Fig. 66A-1-063. $(CH_3)_3NCH_2COO \cdot CaCl_2 \cdot 2H_2O$ (BCCD). p_b vs. T [89Rib2]. Parameter: E_{bias}. p_b: pyroelectric coefficient along b axis. (**a**), (**b**), (**c**) $E_{bias} = 0$. (**d**), (**e**), (**f**) $E_{bias} = 3 \cdot 10^5$ V m^{-1}.

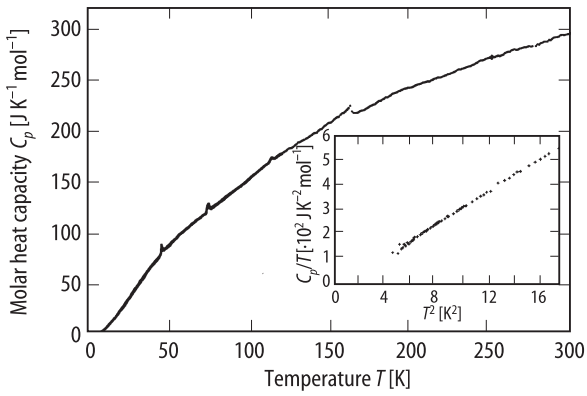

Fig. 66A-1-064. $(CH_3)_3NCH_2COO \cdot CaCl_2 \cdot 2H_2O$ (BCCD). C_p vs. T [90Bri]. C_p: molar heat capacity at constant pressure. Insert: C_p/T vs. T^2 below 4.2 K.

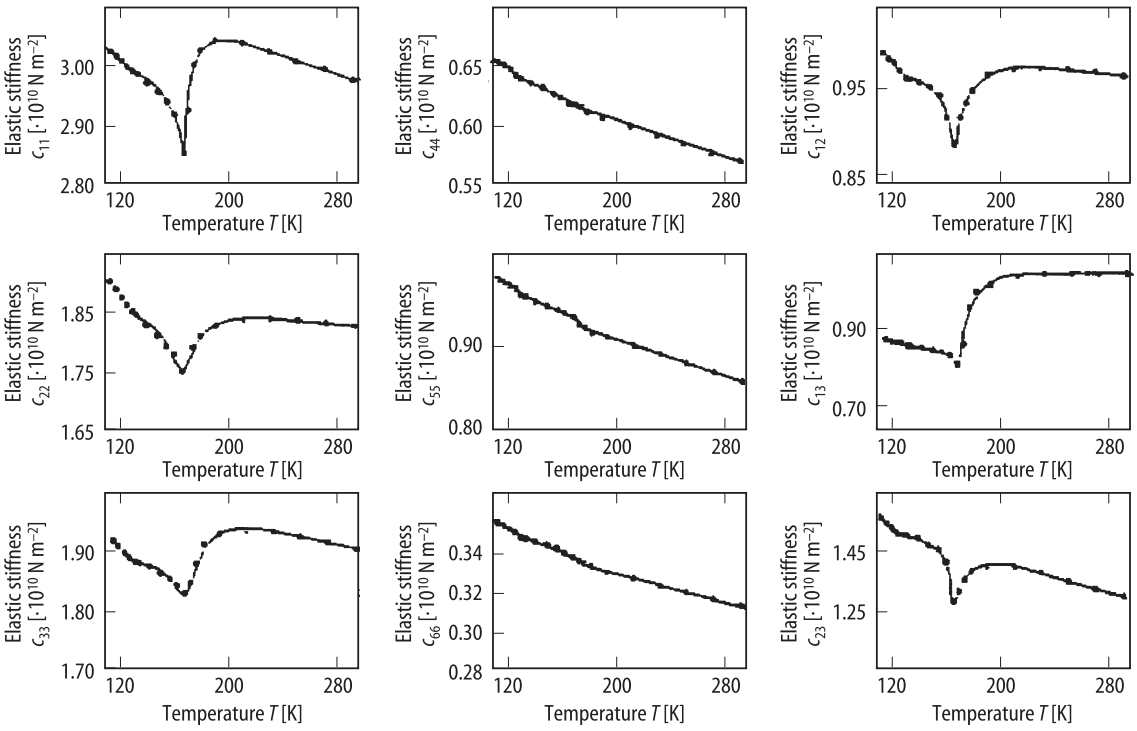

Fig. 66A-1-065. $(CH_3)_3NCH_2COO \cdot CaCl_2 \cdot 2H_2O$ (BCCD). $c_{\lambda\mu}$ vs. T [88Hau]. $c_{\lambda\mu}$: elastic stiffness. $f = 4 \ldots 40$ MHz.

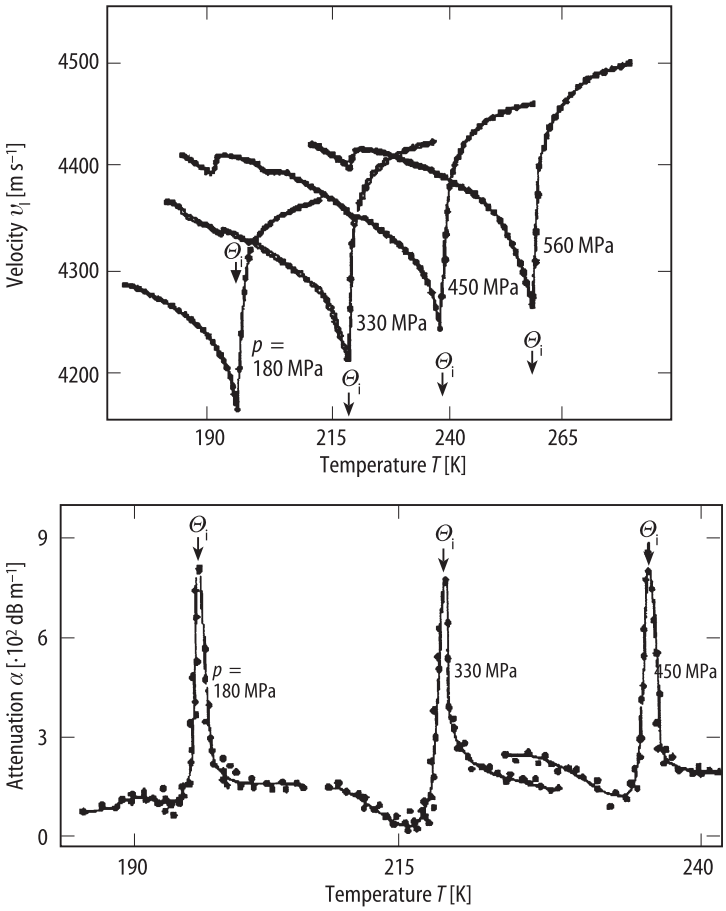

Fig. 66A-1-066. $(CH_3)_3NCH_2COO \cdot CaCl_2 \cdot 2H_2O$ (BCCD). v_l, α vs. T [93Kit]. Parameter: p. v_l, α: velocity and attenuation coefficient of the longitudinal sound wave propagating along the [100] direction. f = 10 MHz.

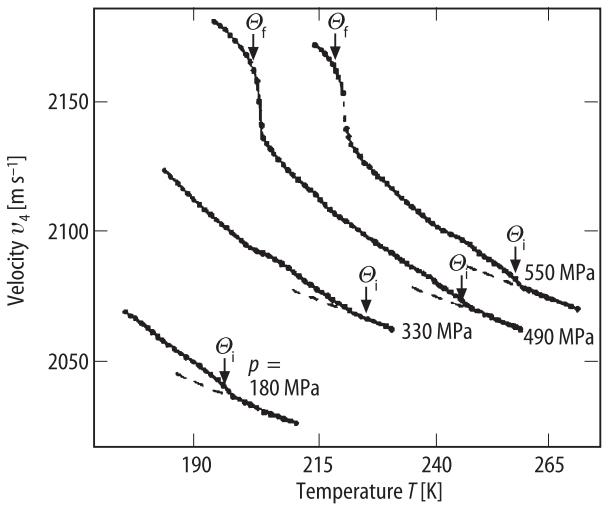

Fig. 66A-1-067. $(CH_3)_3NCH_2COO \cdot CaCl_2 \cdot 2H_2O$ (BCCD). v_4 vs. T [93Kit]. Parameter: p. v_4: velocity of the c_{44} mode sound wave propagating along the b direction with particle displacement in the c direction. f = 10 MHz.

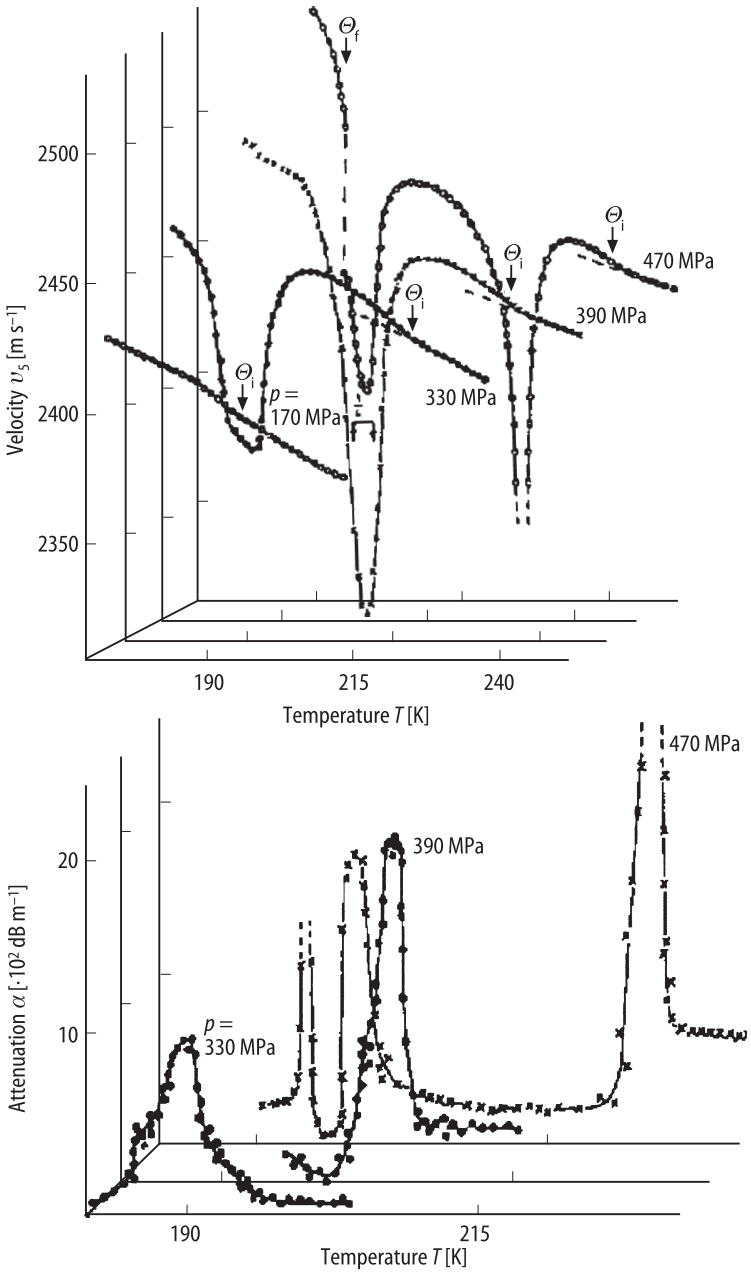

Fig. 66A-1-068. $(CH_3)_3NCH_2COO \cdot CaCl_2 \cdot 2H_2O$ (BCCD). v_5, α vs. T [93Kit]. Parameter: p. v_5, α: velocity and attenuation coefficient of the c_{55} mode sound wave propagating along the a direction with particle displacement in the c direction. f = 10 MHz.

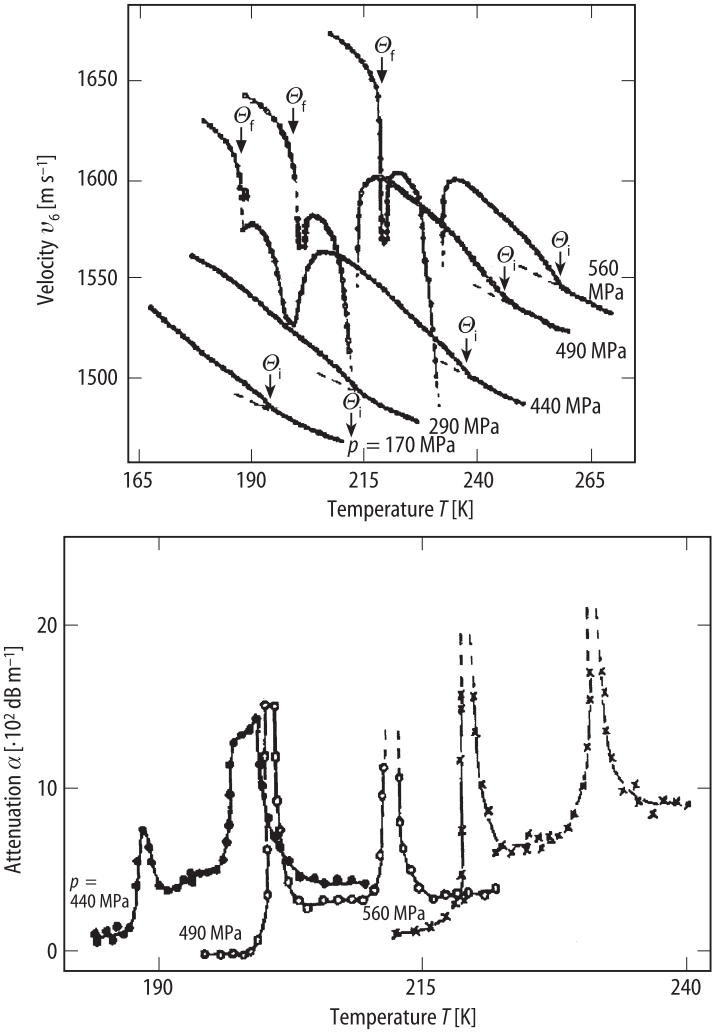

Fig. 66A-1-069. $(CH_3)_3NCH_2COO \cdot CaCl_2 \cdot 2H_2O$ (BCCD). v_6, α vs. T [93Kit]. Parameter: p. v_6, α: velocity and attenuation coefficient of the c_{66} mode sound wave propagating along the a direction with particle displacement in the b direction. f = 10 MHz.

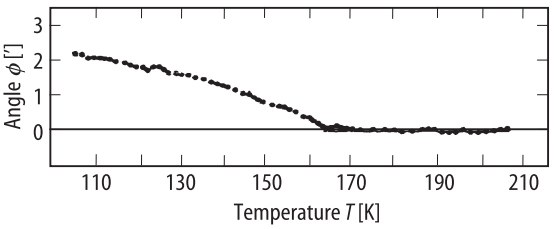

Fig. 66A-1-070. $(CH_3)_3NCH_2COO \cdot CaCl_2 \cdot 2H_2O$ (BCCD). ϕ vs. T [90Kro]. ϕ: rotation angle of optical indicatrix in the ac plane.

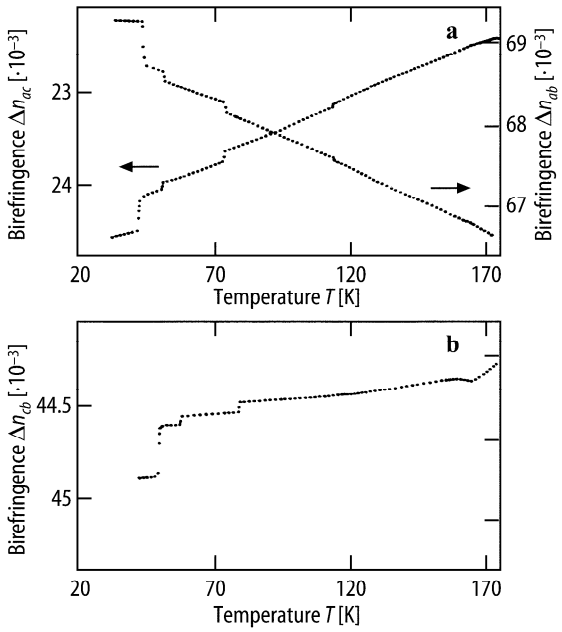

Fig. 66A-1-071. $(CH_3)_3NCH_2COO \cdot CaCl_2 \cdot 2H_2O$ (BCCD). Δn vs. T [90Etx]. $\lambda = 633$ nm. (**a**) Δn_{ac}, Δn_{ab}. (**b**) Δn_{cb}.

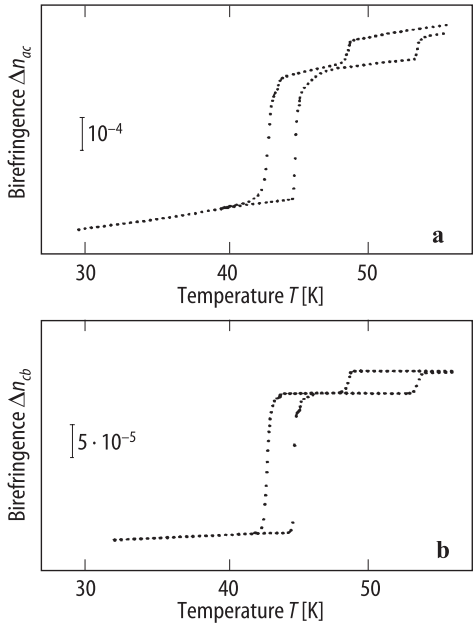

Fig. 66A-1-072. $(CH_3)_3NCH_2COO \cdot CaCl_2 \cdot 2H_2O$ (BCCD). Δn vs. T near Θ_f [90Etx]. $\lambda = 633$ nm. (**a**) Δn_{ac}. (**b**) Δn_{cb}.

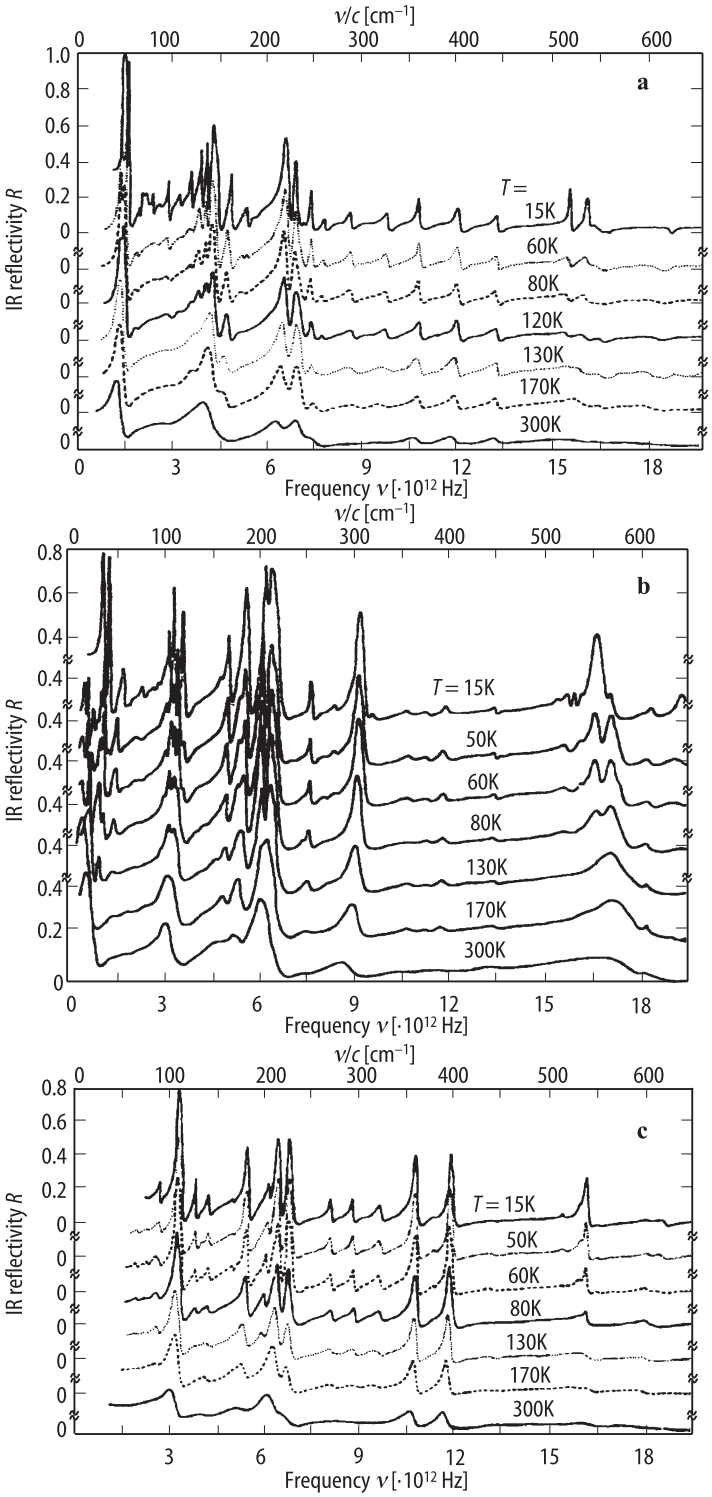

Fig. 66A-1-073. $(CH_3)_3NCH_2COO \cdot CaCl_2 \cdot 2H_2O$ (BCCD). R vs. ν [93Kam]. Parameter: T. R: IR reflectivity. (**a**) $\boldsymbol{E} \parallel \boldsymbol{a}$. (**b**) $\boldsymbol{E} \parallel \boldsymbol{b}$. (**c**) $\boldsymbol{E} \parallel \boldsymbol{c}$.

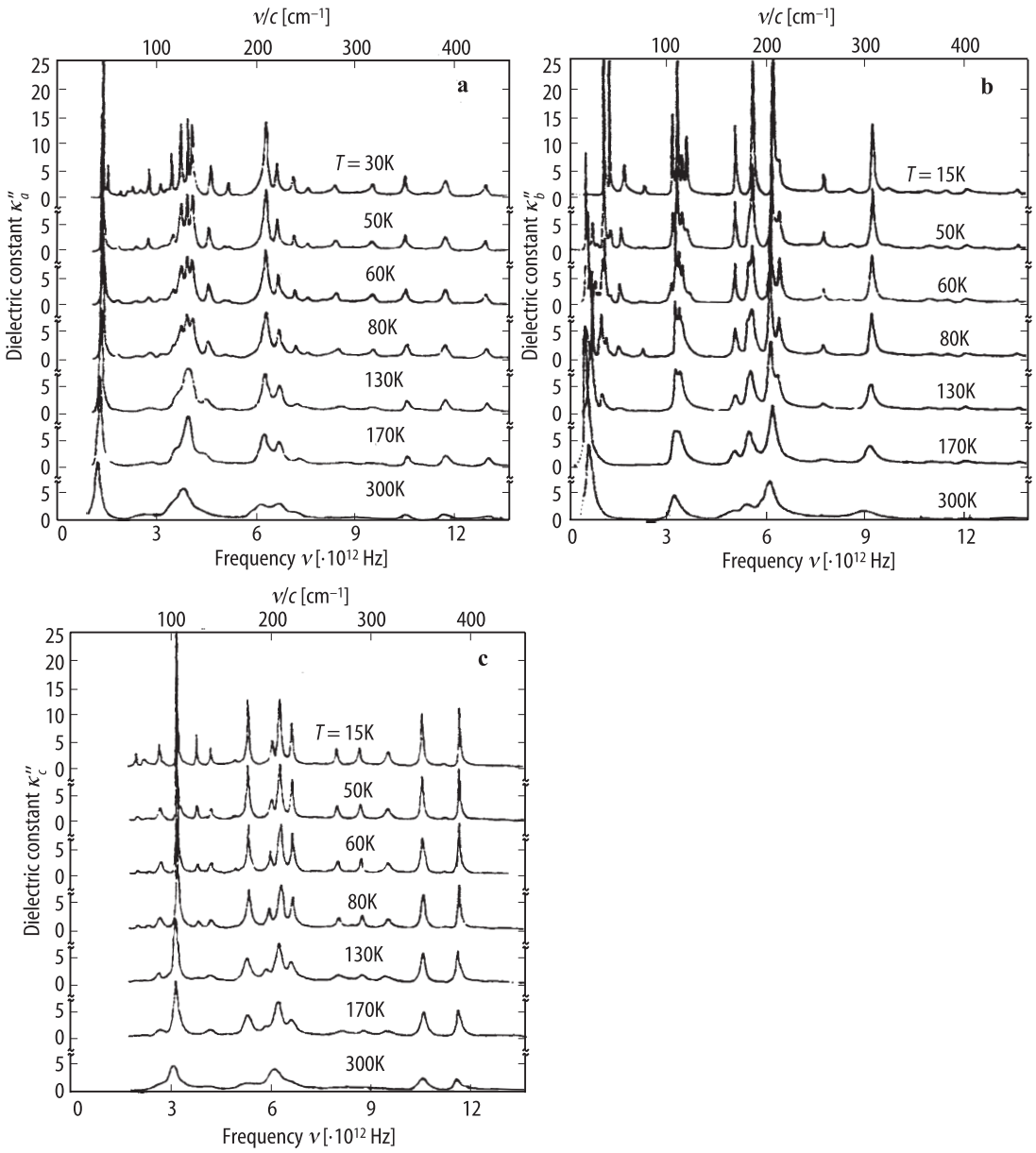

Fig. 66A-1-074. $(CH_3)_3NCH_2COO \cdot CaCl_2 \cdot 2H_2O$ (BCCD). κ'' vs. ν [93Kam]. Parameter: T. κ'' were obtained from IR reflectivity of Fig. 67A-1-073 by Kramers-Kronig relation. (**a**) κ''_a. (**b**) κ''_b. (**c**) κ''_c.

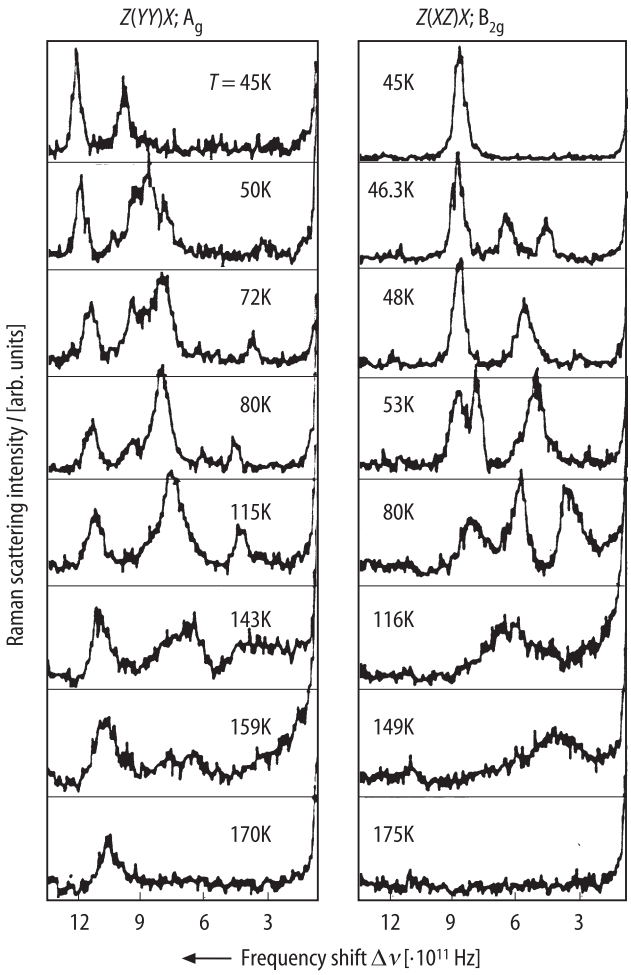

Fig. 66A-1-075. $(CH_3)_3NCH_2COO \cdot CaCl_2 \cdot 2H_2O$ (BCCD). *I* vs. $\Delta\nu$ [88AoR2]. *I*: Raman scattering intensity of the A_g and B_{2g} modes. Parameter: *T*.

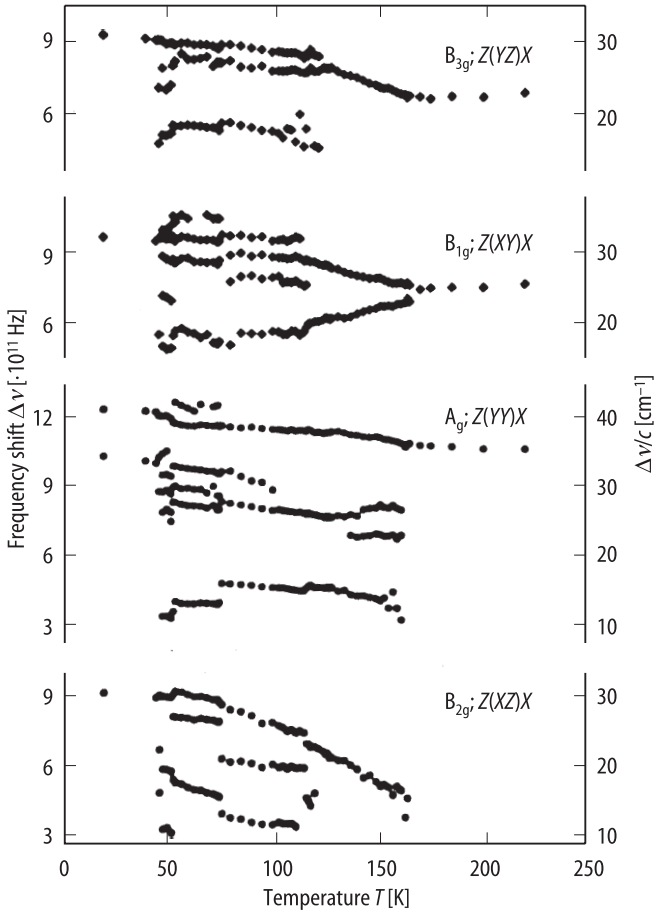

Fig. 66A-1-076. $(CH_3)_3NCH_2COO \cdot CaCl_2 \cdot 2H_2O$ (BCCD). $\Delta\nu$ vs. T [88AoR2]. $\Delta\nu$: Raman scattering frequency shift.

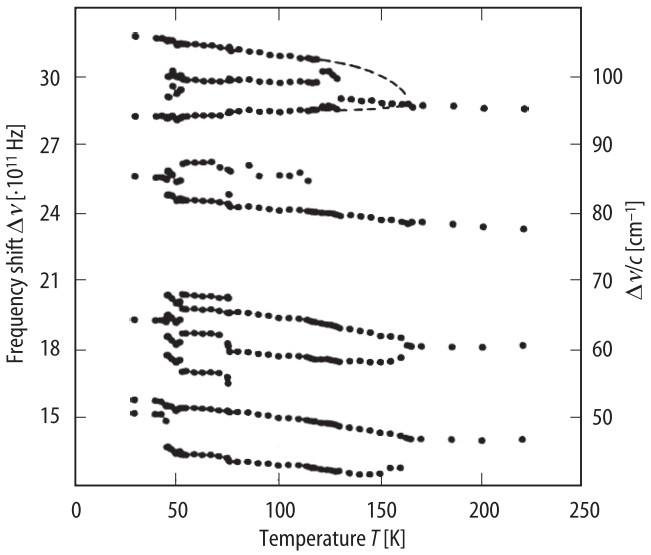

Fig. 66A-1-077. $(CH_3)_3NCH_2COO \cdot CaCl_2 \cdot 2H_2O$ (BCCD). $\Delta\nu$ vs. T [88AoR2]. $\Delta\nu$: Raman scattering frequency shift of the B_{1g} mode.

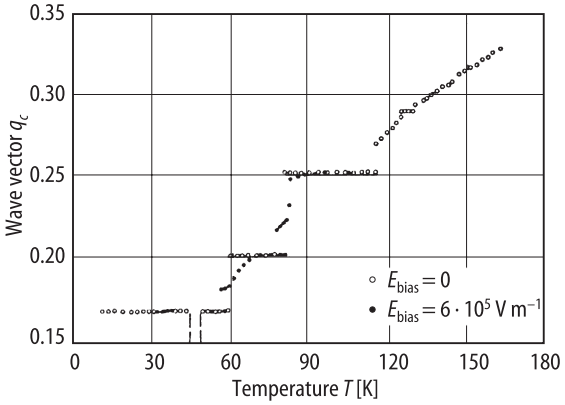

Fig. 66A-1-078. $(CH_3)_3NCH_2COO \cdot CaCl_2 \cdot 2H_2O$ (BCCD). q_c vs. T [85Bri1]. Parameter: E_{bias}. q_c: wave vector of structural modulation in the unit of reciprocal lattice vector c^* determined by X-ray satellite reflection.

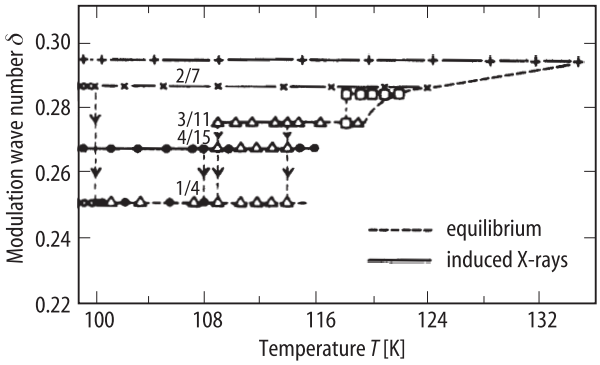

Fig. 66A-1-079. $(CH_3)_3NCH_2COO \cdot CaCl_2 \cdot 2H_2O$ (BCCD). δ vs. T [95Kia]. δ: modulation wave number relative to c^*. Broken line: equilibrium value. Full line: induced by X-ray irradiation.

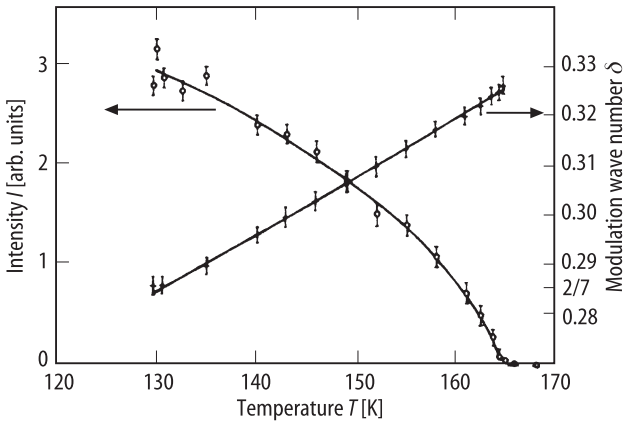

Fig. 66A-1-080. $(CH_3)_3NCH_2COO \cdot CaCl_2 \cdot 2D_2O$. I, δ vs. T [90Cur]. I: intensity of neutron (0, 3, 1–δ) satellite scattering. δ: modulation wave number relative to c^*.

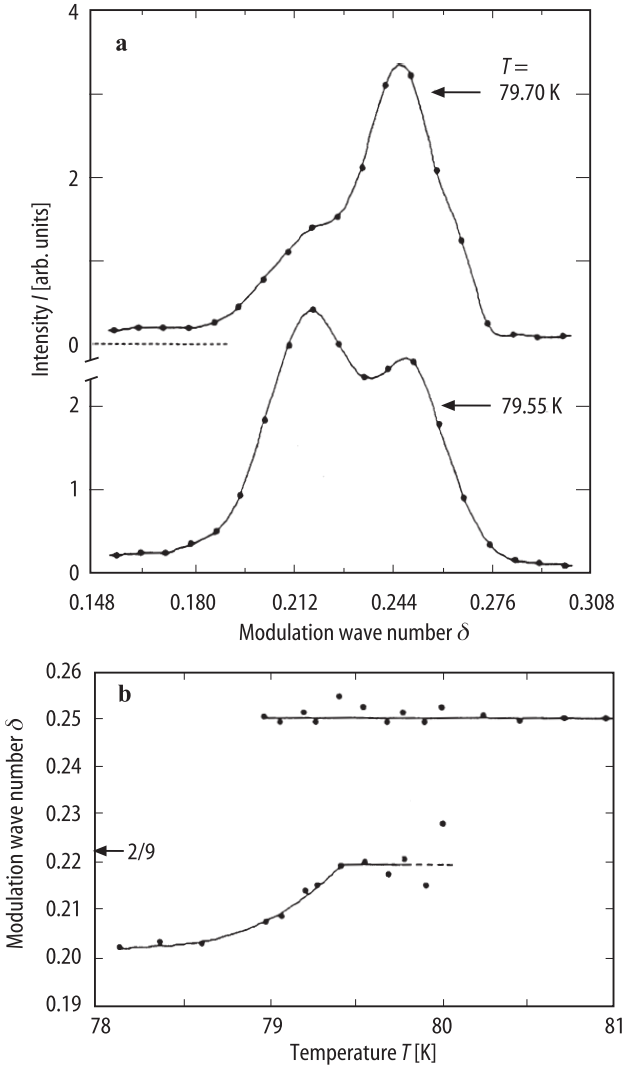

Fig. 66A-1-081. $(CH_3)_3NCH_2COO \cdot CaCl_2 \cdot 2D_2O$. Neutron scattering in the range $\delta = 1/4$ to $\delta = 1/5$ transition [92Alm]. δ: modulation wave number relative to c^*. (**a**) I vs. δ. Parameter: T. I: intensity of satellite. (**b**) δ vs. T on cooling, showing the coexistence of two kinds of satellites.

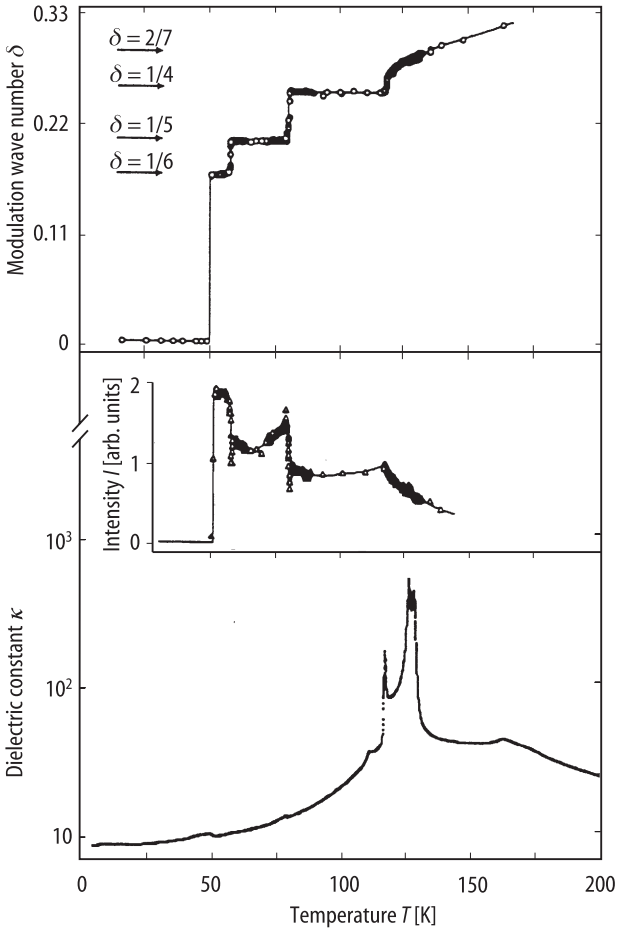

Fig. 66A-1-082. $(CH_3)_3NCH_2COO \cdot CaCl_2 \cdot 2D_2O$. δ, I, κ vs. T [92Alm]. δ: modulation wave number relative to c^*. I: neutron scattering intensity of satellite.

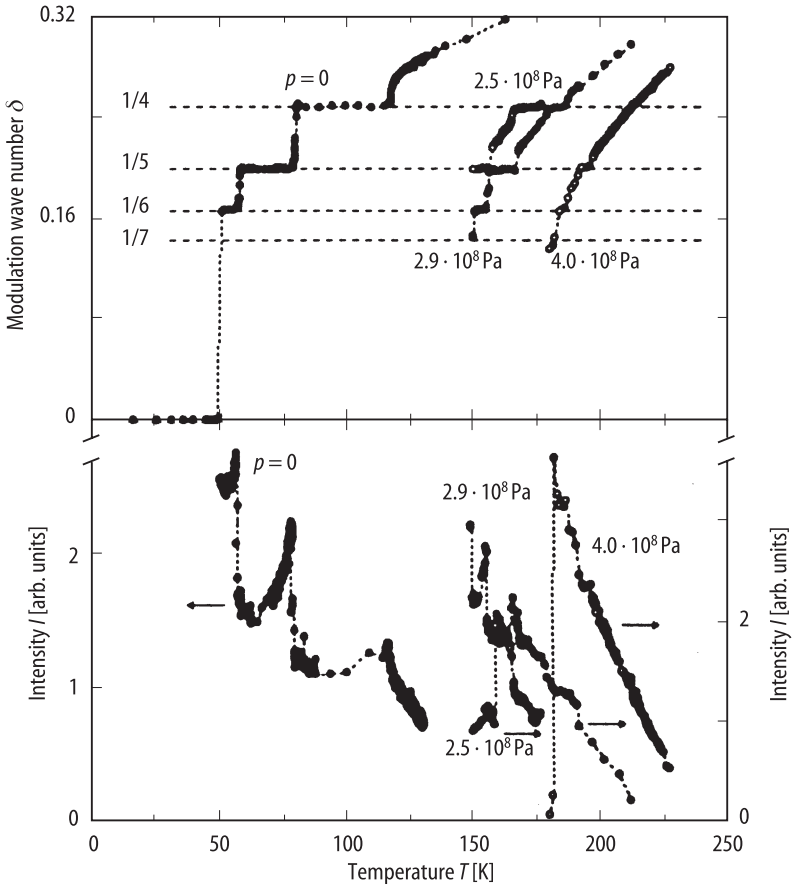

Fig. 66A-1-083. $(CH_3)_3NCH_2COO \cdot CaCl_2 \cdot 2D_2O$. δ, I vs. T [93Cha1]. Parameter: p. δ: modulation wave number relative to c^*. I: integrated neutron scattering intensity of satellites at $(0, 6, \pm \delta)$.

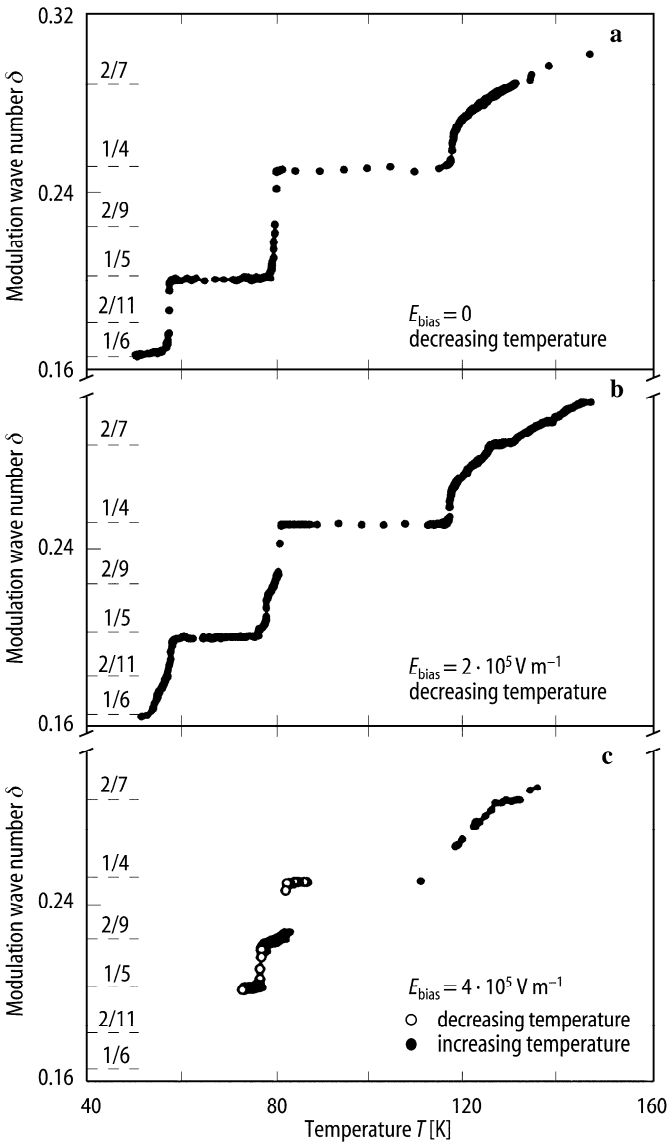

Fig. 66A-1-084. $(CH_3)_3NCH_2COO \cdot CaCl_2 \cdot 2D_2O$. δ vs. T [93Cha2]. Parameter: E_{bias}. δ: modulation wave number relative to c^*. (**a**) $E_{bias} = 0$. (**b**) $E_{bias} = 2 \cdot 10^5$ V m^{-1}. (**c**) $E_{bias} = 4 \cdot 10^5$ V m^{-1}.

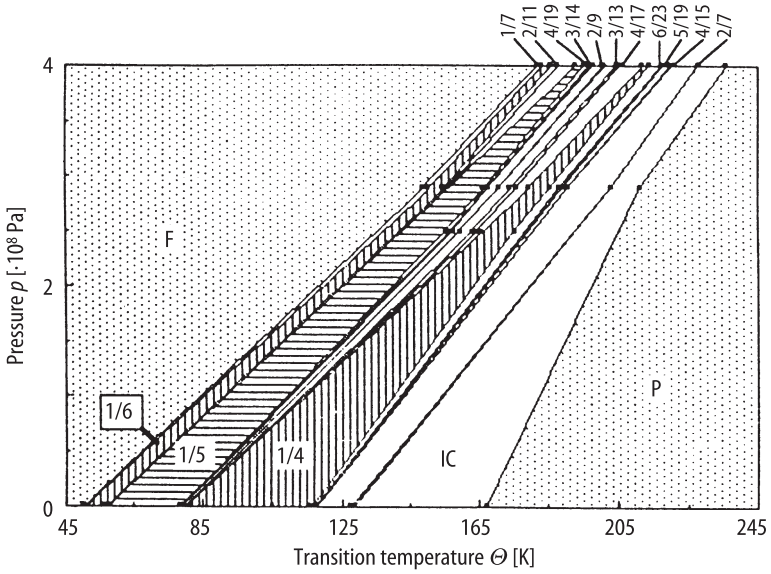

Fig. 66A-1-085. $(CH_3)_3NCH_2COO \cdot CaCl_2 \cdot 2D_2O$. $p - \Theta$ phase diagram [93Cha1]. P: paraelectric region. F: ferroelectric region. Hatched area: commensurately modulated phase. Open area: incommensurately modulated phase. Fractions indicate the wave numbers in the units of c^* of structure modulation in the commensurately modulated phase.

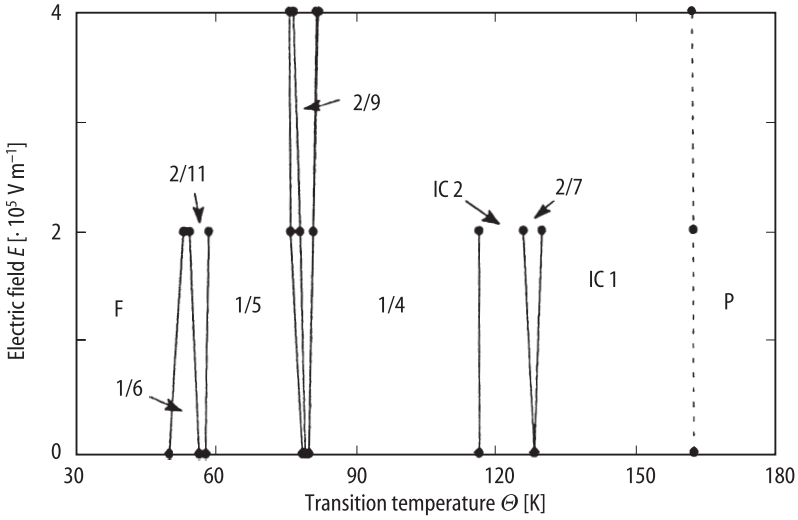

Fig. 66A-1-086. $(CH_3)_3NCH_2COO \cdot CaCl_2 \cdot 2D_2O$. $E - \Theta$ phase diagram from neutron data [93Cha2]. P: paraelectric region. F: ferroelectric region. IC: incommensurately modulated phase. Fractions indicate the wave numbers in the units of c^* of structure modulation in the commensurately modulated phase.

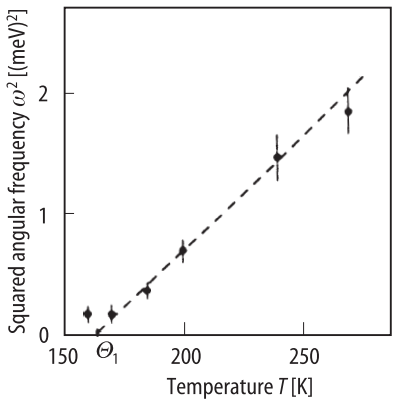

Fig. 66A-1-087. $(CH_3)_3NCH_2COO \cdot CaCl_2 \cdot 2D_2O$. ω^2 vs. T [90Cur]. ω: soft mode angular frequency at $\boldsymbol{k}$ = (0, 3, 0.7).

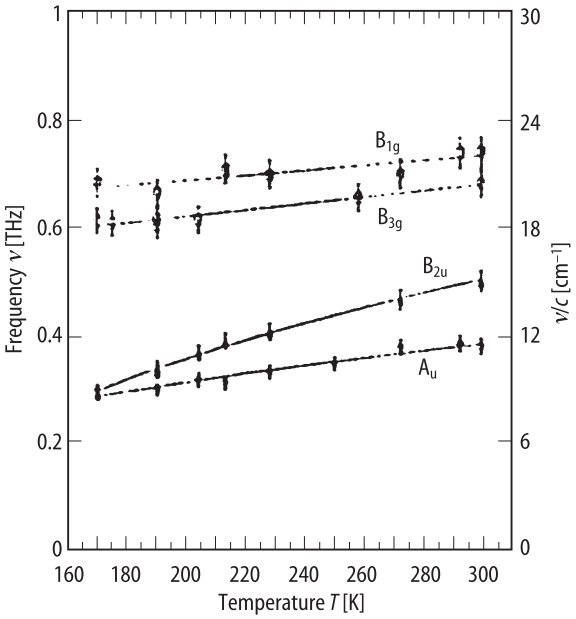

Fig. 66A-1-088. $(CD_3)_3NCD_2COO \cdot CaCl_2 \cdot 2D_2O$ (DBCCD). ν vs. T in phase I [94Kam]. ν: frequencies of Γ-point modes.

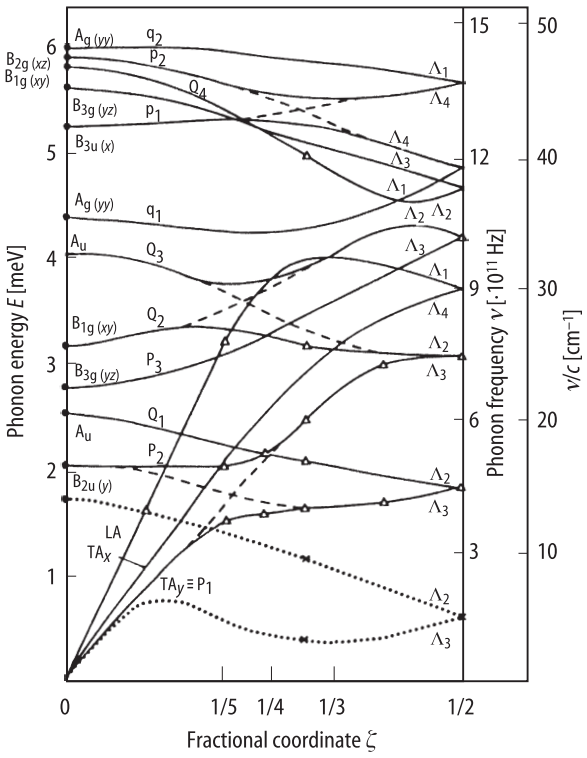

Fig. 66A-1-089. $(CH_3)_3NCH_2COO \cdot CaCl_2 \cdot 2D_2O$. E, ν vs. ζ [90Cur]. E: phonon energy. ν: phonon frequency. ζ: fractional coordinate in the reciprocal space along c^*. Open triangle, cross: neutron scattering [90Cur]. Full circle: infrared [88AoR1, 86Vol, 88Gon] and Raman [88AoR2] scattering. Solid lines: $T = 270$ K. Dotted lines: $T = 170$ K.

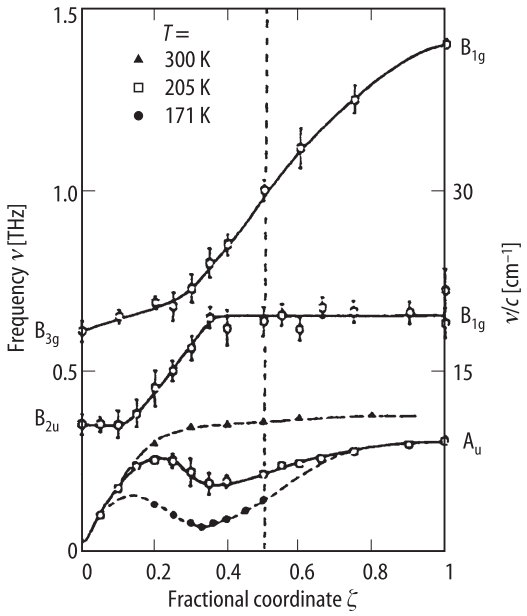

Fig. 66A-1-090. $(CH_3)_3NCH_2COO \cdot CaCl_2 \cdot 2D_2O$ (DBCCD). ν vs. ζ in phase I [94Kam]. Parameter: T. ν: frequency of low energy phonon branch. ζ: fractional coordinate in the reciprocal space along c^*.

References

84Rot Rother, H.J., Albers, J., Klöpperpieper, A.: Ferroelectrics **54** (1984) 107.
85Bri1 Brill, W., Ehses, K.H.: Jpn. J. Appl. Phys. **24** (1985) Suppl. 24–2, 826.
85Bri2 Brill, W., Schildkamp, W., Spilker, J.: Z. Kristallogr. **172** (1985) 281.
85Klo Klöpperpieper, A., Rother, H.J., Albers, J., Müser, H.E.: Jpn. J. Appl. Phys. **24** (1985) Suppl. 24–2, 829.
86Vol Volkov, A.A., Goncharov, Yu.G., Kozlov, G.V., Albers, J., Petzelt, J.: Pis'ma Zh. Eksp. Teor. Fiz. **44** (1986) 469; JETP Lett. (English Tranls.) **44** (1986) 603.
88AoR1 Ao, R., Schaack, G.: Ferroelectrics **80** (1988) 105.
88AoR2 Ao, R., Schaack, G.: Indian J. Pure Appl. Phys. **26** (1988) 124.
88Gon Goncharov, Yu.G., Kozlov, G.V., Volkov, A.A., Albers, J., Petzelt, J.: Ferroelectrics **80** (1988) 221.
88Hau Haussühl, S., Liedtke, J., Albers, J., Klöpperpieper, A.: Z. Phys. B **70** (1988) 219.
88Rib1 Ribeiro, J.L., Chaves, M.R., Almeida, A., Albers, J., Klöpperpieper, A., Müser, H.E.: Ferroelectrics Lett. **8** (1988) 135.
88Rib2 Ribiro, J.L., Fayet, J.C., Emery, J., Pézeril, M., Albers, J., Klöpperpieper, A., Almeida, A., Chaves, M.R.: J. Phys. (Paris) **49** (1988) 813.
89Fuj Fujimoto, M., Kotake, Y.: J. Chem. Phys. **90** (1989) 532.
89Rib1 Ribeiro, J.L., Chaves, M.R., Almeida, A., Albers, J., Klöpperpieper, A., Müser, H.E.: J. Phys. Condens. Matter **1** (1989) 8011.
89Rib2 Ribeiro, J.L., Chaves, M.R., Almeida, A., Albers, J., Klöpperpieper, A., Müser, H.E.: Phys. Rev. B **39** (1989) 12320.
89Unr Unruh, H.-G., Hero, F., Dvorák, V.: Solid State Commun. **70** (1989) 403.
90AoR Ao, R., Lingg, G., Schaack, G., Zoller, M.: Ferroelectrics **105** (1990) 391.
90Bri Brill, W., Gmelin, E., Ehses, K.H.: Ferroelectrics **103** (1990) 25.
90Cur Currat, R., Legrand, J.E., Kamba, S., Petzelt, J., Dvorak, V., Albers, J.: Solid State Commun. **75** (1990) 545.
90Eme Emery, J., De Azevedo, J.C., Fayet, J.C., Chaves, M.R., Albers, J., Klöpperpieper, A., Ribeiro, J.L., Almeida, A.: Ferroelectrics **105** (1990) 373.
90Etx Etxebarria, J., Pérez-Mats, J.M., Breczewski, T., Arnoiz, A.R.: Solid State Commun. **76** (1990) 461.
90Fre Freitag, O., Unruh, H.-G.: Ferroelectrics **105** (1990) 357.
90Kro Kroupa, J., Albers, J., Ivanov, N.R.: Ferroelectrics **105** (1990) 345.
90Rib1 Ribeiro, J.L., Chaves, M.R., Almeida, A., Müser, H.E., Albers, J., Klöpperpieper, A.: Ferroelectrics **105** (1990) 396.
90Rib2 Ribeiro, J.L., Chaves, M.R., Almeida, A., Müser, H.E., Albers, J., Klöpperpieper, A.: Ferroelectrics **105** (1990) 363.
91Cha Chaves, M.R., Almeida, A., Carvalho, P.S., Ribeiro, J.L., Müser, H.E., Albers, J., Klöpperpieper, A.: Phys. Rev. B **43** (1991) 11162.
91Met Metz, H., Schaack, G., Schmitt, M., Windsch, W.: Phys. Status Solidi (a) **126** (1991) K73.
91Rib1 Ribeiro, J.L., Chaves, M.R., Almeida, A., Müser, H.E., Albers, J., Klöpperpieper, A.: Phys. Status Solidi (b) **163** (1991) 503.
91Rib2 Ribeiro, J.L., Chaves, M.R., Almeida, A., Müser, H.E., Albers, J., Klöpperpieper, A.: Phys. Status Solidi (b) **163** (1991) 511.
91Wil Wilhelm, H., Unruh, H.-G.: Z. Kristallogr. **195** (1991) 75.
91Zun Zúñiga, F.J., Ezpeleta, J.M., Pérez-Mato, J.M., Paciorek, W., Madaringa, G.: Phase Transitions **31** (1991) 29.
92Alm Almeida, A., Chaves, M.R., Kiat, J.M., Schneck, J., Schwarz, W., Toledano, J.C., Ribeirs, J.L., Klöpperpieper, A., Müser, M.E., Albers, J.: Phys. Rev. B **45** (1992) 9576.
92Cha Chaves, M.R., Almeida, A., Carvalho, P.S.: Data cited in [92Alm].
92Ezp Ezpeleta, J.M., Zúñiga, F.J., Pérez-Mato, J.M., Paciorek, W.A., Breczewski, T.: Acta Crystallogr. Sect. B **48** (1992) 261.
92Hac Häcker, U., Holzer, K.-P., Michel, D., Petersson, J.: Solid State Commun. **83** (1992) 81.

92Hei Heidler, R., Windsh, W.: Chem. Phys. Lett. **193** (1992) 147.
92LeM Le Maire, M., Lingg, G., Schaack, G., Schmitt-Lewen, M., Strauss, G., Klöpperpieper, A.: Ferroelectrics **125** (1992) 87.
93Alm Almeida, A., Chaves, M.R., Ribeiro, J.L., Klöpperpieper, A., Müser, H.E., Albers, J.: Ferroelectrics **141** (1993) 13.
93Cha1 Chaves, M.R., Kiat, J.M., Schwarz, W., Schneck, J., Almeida, A., Klöpperpieper, A., Müser, H.E., Albers, J.: Phys. Rev. B **48** (1993) 5852.
93Cha2 Chaves, M.R., Almeida, A. Toledano, J.C., Schneck, J., Kiat, J.M., Schwarz, W., Ribeiro, J.L., Klöpperpieper, A., Albers, J., Müser, H.E.: Phys. Rev. B **48** (1993) 13318.
93Kam Kamba, S., Dvorák, V., Petzelt, J., Goncharov, Yu.G., Volkov, A.A., Kozlov, G.V.: J. Phys. Condens. Matter **5** (1993) 4401.
93Kit Kityk, A.V., Soprunyuk, V.P., Vlohk, O.G., Sveleba, S.A., Czapla, Z.: J. Phys. Condens. Matter **5** (1993) 7415.
94Ill Illing, M., Schaack, G., Schmitt-Lewen, M.: Ferroelectrics **155** (1994) 341.
94Kam Kamba, S., Petzelt, J., Zelezny, V., Smutny, F., Dvorák, V., Hlinka, J., Quilichini, M., Volkov, A.A., Gorshunov, B.P., Kozlov, G.V., Currat, R., Legrand, J.F.: Ferroelectrics **159** (1994) 97.
94LeM Le Maire, M., López ayala, A., Schaack, G., Klöpperpieper, A., Metz, H.: Ferroelectrics **155** (1994) 335.
95Ban Banya, J., Sobiestianskas, R., Brilingas, A.: Phys. Status Solidi (a) **147** (1995) K103.
95Hol Holzer, K.-P., Häcker, U., Petersson, J., Michel, D., Kluthe, S.: Solid State Commun. **94** (1995) 275.
95Kia Kiat, J.M., Calvarin, G., Chaves, M.R., Almeida, A., Klöpperpieper, A., Albers, J.: Phys. Rev. B **52** (1995) 789.
95Sve Sveleba, S.A., Kapustianik, V., Polovinko, J., Bublyk, M., Styrkowiec, R., Czapla, Z.: Phys. Status Solidi (a) **147** (1995) 257.